Thesis for the Degree of Doctor of Philosophy

Two-Electron Excitations in Negative Ions

Anton O. Lindahl

UNIVERSITY OF GOTHENBURG

Department of Physics
University of Gothenburg
Göteborg 2011

Two-Electron Excitations in Negative Ions
Anton O. Lindahl

ISBN: 978-91-628-8363-8
Electronic version available at http://hdl.handle.net/2077/26757

Typeset using LaTeX
Figures created using MATLAB and Powerpoint. All figures are the original work by the author.

Cover picture: Artists impression of photodetachment of K^-. Created by Alfred Lindahl.

Department of Physics
University of Gothenburg
SE-412 96 Göteborg, Sweden
Phone: +46 (0)31 786 0000

Printed by Kompendiet
Göteborg, Sweden 2011

Two-Electron Excitations in Negative Ions

Anton O. Lindahl

Department of Physics
University of Gothenburg
Göteborg, Sweden

Abstract

The main goal of this work has been to increase the knowledge of electron-electron correlation through experimental studies of negative ions. Negative ions are atoms or molecules to which an extra electron has been attached. Due to the energy sharing between the electrons, the effects of electron interactions, and thus electron-electron correlation, are relatively large in these systems. Comparisons of experimental data and results from *ab initio* many-body calculations can therefore serve as sensitive tests of our knowledge of these correlation effects.

This thesis describes experimental investigations of fundamental properties of atomic negative ions. Photodetachment experiments have been performed with collinearly merged laser- and ion-beams. A new threshold behaviour have been observed in photodetachment of K^- into the $K(5\,^2G)$ channel. A semi-classical model has been developed, which qualitatively describes the behaviour as a result of the large and negative polarisability of the $5\,^2G$ state. Partial cross sections for K^- and Cs^- photodetachment to highly excited states in the residual atom have been measured. Two previously unobserved resonances have been identified in K^- below the $K(7\,^2P)$ channel opening, while a rich spectrum of resonances was observed in Cs^- below the $Cs(10\,^2P_{1/2,3/2})$ thresholds.

Improved values for the electron affinities of W and P and the fine structure intervals of P^- are presented. Moreover, the binding energy of the previously unobserved $^2S_{1/2}$ state in Pt^- has been determined, and photodetachment from a previously unknown bound state in W^- has been observed.

The experiments were made possible by extensive development of the experimental facility at GUNILLA (Göteborg University Negative Ion Laser LAboratory). A state-selective detection scheme utilizing resonance ionisation has been developed. It is based on excitation to a Rydberg state, which is field-ionised in an inhomogeneous field. The produced positive ion is subsequently detected with a position-sensitive detector. The resolution of the mass spectrometer has been substantially improved, which proved important in the W^- and Pt^- measurements.

Contents

Appended Papers

This thesis is based on the scientific work presented in the following papers. The papers are printed as appendices and are referred to by Roman numerals in the text.

I Ion optical design of a collinear laser-negative ion beam apparatus
C. Diehl, K. Wendt, A. O. Lindahl, P. Andersson, and D. Hanstorp
Review of Scientific Instruments, ***82****, 053302 (2011)*
doi: 10.1063/1.3587617

II The electron affinity of phosphorus
P. Andersson, A. O. Lindahl, C. Alfredsson, L. Rogström, C. Diehl, D. J. Pegg and D. Hanstorp
Journal of Physics B: Atomic, Molecular and Optical Physics ***40****, 4097 (2007)*
doi: 10.1088/0953-4075/40/20/010

III The electron affinity of tungsten
A. O. Lindahl, P. Andersson, C. Diehl, O. Forstner, P. Klason, and D. Hanstorp
The European Physics Journal D, ***60****, 219 (2010)*
doi: 10.1140/epjd/e2010-00199-y

IV Observation of the $^2S_{1/2}$ metastable state in Pt^-
P. Andersson, A. O. Lindahl, D. Hanstorp, and D. J. Pegg
Physical Review A, ***79****, 022502 (2009)*
doi: 10.1103/PhysRevA.79.022502

V Experimental studies of partial photodetachment cross sections in K^- below the $K(7\,^2P)$ threshold
A. O. Lindahl, J. Rohlén, H. Hultgren, I. Yu. Kiyan, D. J. Pegg, C. W. Walter, and D. Hanstorp
In manuscript

VI Photodetachment in a repulsive potential
A. O. Lindahl, J. Rohlén, H. Hultgren, I. Yu. Kiyan, D. J. Pegg, C. W. Walter, and D. Hanstorp
Submitted to Physical Review Letters

VII Observation of overlapping resonances below the $10\,^2P_{1/2,3/2}$ states in photodetachment of Cs^-
A. O. Lindahl, J. Rohlén, H. Hultgren, D. J. Pegg, C. W. Walter, and D. Hanstorp
In manuscript

The main contributions made by me and the other authors to the above-listed papers are the following:

I played a major part in the discussions that led to the final design presented in paper **I**. CD performed calculations and simulations, which were used as a basis for the discussions. I had the main responsibility for the design of the vacuum system. I assembled the apparatus together with CD. I wrote the first draft of the manuscript.

PA was responsible for paper **II**. I participated in the experiment and the data analysis.

I had the main responsibility for the experiment presented in paper **III**. The background investigation was performed by me and PA. I wrote the paper.

PA did most of the experimental work for paper **IV**. I developed the technique of measuring photodetachment signals together with a mass spectrum and took part in the analysis. PA wrote the paper.

I constructed the set-up used to perform the experiments in papers **V**, **VI** and **VII**. I had the responsibility for and knowledge of all parts of the experiment and the data acquisition system (hardware and software). All authors had their share of night shifts. JR developed the first version of the data analysis code. I performed the data analysis. The threshold model described in paper **VI** was developed by IK. JR wrote the first draft of paper **VII**. I was responsible for writing papers **V**, **VI** and **VII**.

Related Papers

During my time as a Ph.D. student I have, in addition to the seven papers that forms the basis of my thesis, published another six papers in the field of negative ions. Five of these papers are related to applications in mass spectrometry. The sixth paper is a study of electron impact detachment on a molecular negative ion. The scientific work presented in these papers is outside the scope of this thesis. These papers, however, are listed below in order to give a broader view of my work. A full and updated list of the publications can be found on ResearcherID.com, my RID is A-5366-2011.

- The electronic structure of HfF_5^- and WF_5^-
  H. Chen, P. Andersson, A. O. Lindahl, and D. Hanstorp
  Chemical Physics Letters, ***511****, 196 (2011)*

- Depletion of the excited state population in negative ions using laser photodetachment in a gas-filled RF quadrupole ion guide
  A. O. Lindahl, D. Hanstorp, O. Forstner, N. D. Gibson, T. Gottwald, K. Wendt, C. C. Havener, and Y. Liu
  Journal of Physics B: Atomic, Molecular and Optical Physics, ***43****, 115008 (2010)*

- Nearly complete isobar suppression by photodetachment
  P. Andersson, A. O. Lindahl, D. Hanstorp, C. C. Havener, Yun Liu, and Yuan Liu
  Journal of Applied Physics, ***107****, 026102 (2010)*

- Isobar selective laser photodetachment in trace element analysis
  P. Andersson, O. Forstner, D. Hanstorp, A. O. Lindahl, and K. Wendt
  AIP Conference Proceedings, ***1104****, 53 (2009)*

- Isobar suppression in AMS using laser photodetachment
  O. Forstner, P. Andersson, C. Diehl, R. Golser, D. Hanstorp, W. Kutschera, A. Lindahl, A. Priller, P. Steier, and A. Wallner
  Nuclear Instruments and Methods in Physics Research Section B: Beam Interactions with Materials and Atoms, ***266****, 4565 (2008)*

- Experimental investigation of electron impact on Si_2^-
  A. O. Lindahl, P. Andersson, G. F. Collins, D. Hanstorp, D. J. Pegg, M. Danielsson, W. D. Geppert, M. Hamberg, R. D. Thomas, V. Zhaunerchyk, C. Diehl, N. D. Gibson, and A. Källberg
  Physical Review A, ***77****,022710 (2008)*

Preface

I have always wanted to understand the world, often asking the questions "How?" and "Why?". When I was only five years old, my father explained Archimedes' principle to me when I was playing in the bathtub. Although I have always had the interest, it has not always been obvious to me that I should take the road towards a career in science. In hindsight, however, the path from the bathtub to this Ph.D. thesis seems rather straight. I guess most people who know me are not at all surprised by my choices.

I have spent five and a half years as a Ph.D. student, and I have enjoyed most of it. Even the long data acquisition shifts had their special appeal. Not to mention the night when we, more or less, stumbled on the threshold behaviours that are presented in paper V. These observations fitted exactly into my expectations of how scientific discoveries are made: with a lot of hard work and some good luck.

There have, however, been a few difficult days. Moments when I have been 100% sure that the experiment would never work. But fortunately, I was wrong. Everything came together in the end and I managed to get some good results.

This thesis marks the endpoint of my time as a Ph.D. student. It is a summary of what I have done but it is far from the full story. The material presented in the thesis is selected in order to tell a single story. A story from P to Cs that is gradually increasing in both experimental and physical complexity. The appended papers are important parts of this thesis. The summary serves the purpose of linking together the individual papers and giving an introduction to the experiments for a person not familiar with the field. I have kept the level of detail in the summary at a minimum, while more details are given in the papers.

Experimental physics requires a thorough understanding of the basic principles behind your investigations. You need to understand the physics in order to ask the interesting and relevant questions, and to be able to set up a functioning experiment. Working in a laboratory is, however, not only about knowing the principles of the experiments. Experimental science is a craft. There are hundreds of parameters in an experiment. Each of them has to be set just right. It is possible to learn how to handle each single degree of freedom in a few months, in order to reproduce something you have done before. To do something new, however, you need to know the interplay between your parameters. You also need to have a feeling for what you do, and the feeling should include both your head and your hands. A lot of the things I have learned as a Ph.D. student are things belonging to the craft of experimental physics. These things are not explicitly treated in the text, but keep this in mind when you read the thesis. I hope you will enjoy it!

Göteborg, September 2011
Anton O. Lindahl

CHAPTER 1

Introduction

Our understanding of the physics of atoms and molecules stems from developments in the first decades of the twentieth century. The Bohr model of the atom, which was presented as early as 1913, is still used as a simple, easy to picture, model for one-electron atomic systems. In order to describe multi-electron systems, however, a quantum mechanical treatment is needed.

The most common formalism used in quantum mechanics is based on the Schrödinger equation (from 1926) and its relativistic counterpart, the Dirac equation (from 1928). By solving these equations we can, in principle, describe and understand the atomic world. The fundamental problem is that these equations can only be solved analytically for a few very simple cases. In most atomic systems approximations must be introduced and the resulting equations, describing the structure and dynamics, are often solved numerically. There are many different approaches to such calculations and all of them are based on specific simplifications and assumptions. One simplification, that works rather well for atoms, is the independent particle model. It is based on the approximation that each electron experiences the mean field created by the nucleus and the other electrons. In other words, the motion of the electrons are uncorrelated.

A negative ion is a quantum mechanical system with a net negative charge as a result of a neutral atom or molecule capturing an additional electron. The binding energy of the extra electron in a negative ion is typically much smaller than binding energy in the corresponding neutral system. The outermost electron in an atomic or molecular system experiences a net attractive force that is the combination of an attractive electron-nucleus force and a re-

pulsive electron-electron force. In a negative ion, the nucleus is well shielded by a full compliment of atomic electrons. This makes the electron-electron force relatively more important. In order for the extra electron to experience at net attractive force the motion of the electrons must be correlated. A consequence of this is that the independent particle model does not do well in describing negative ions. Experimental studies of the structure and dynamics of negative ions can therefore teach us a lot about the nature of electron-electron correlation. Comparisons of experimental results with calculations provide valuable tests of our general theoretical understanding of correlated many-body systems.

The simplest negative ion is H^-, consisting of a singly charged nucleus and two electrons. Much effort has been invested in studies of the binding energy of H^-, both theoretically [1] and experimentally [2]. Doubly excited states of negative ions in general, and H^- in particular, have also attracted a lot of attention [3–6]. States with two highly excited electrons are even more sensitive to electron-electron correlation than negative ion ground states. One can think of the extra electron moving in the field of an excited parent atom. Unfortunately, in the prototypical ion, H^-, the level of excitation of doubly excited states is very high and traditional light sources cannot be used to access them. Due to the difficult experimental requirements, many studies have instead focused on quasi two-electron systems such as the alkali metal negative ions [7–10]. He^-, a fundamental three-electron system has also been thoroughly investigated [11, 12].

Our knowledge of negative ions does, however, date back much further than the above mentioned work. As early as 1913, J. J. Thomson observed what he described as "negatively electrified atoms" [13]. Twenty years later, Wildt proposed that H^- has a big influence on the infrared part of the solar spectrum [14, 15]. This proposal spurred Branscomb *et al.* to work on experiments that led to the first photodetachment cross section studies of H^- [16, 17]. Branscomb also studied O^- and performed the first determination of an electron affinity with a photodetachment threshold measurement in 1955 [18]. Branscomb was one of the pioneers in the experimental field of photodetachment. On the other hand, Sir H. Massey, a theorist, is known for his calculations of negative ion structure. In 1938, Massey published the first edition of *Negative ions*, a book containing almost all information on negative ions at the time. The third edition of *Negative Ions* was published in 1976 [19] and is still an important comprehensive work on the subject of negative ions. Today, the electron affinities of most elements are known and compilations of binding energies in atomic [20] as well as molecular [21] negative ions exist.

The interest in negative ions extends far beyond fundamental research.

For example, negative ions are commonly found in aqueous environments. The strong interaction with the polar water molecules stabilises the otherwise fragile ions. But the ion properties are also changed by the interaction. In gas phase, the most important application of negative ions nowadays is in plasma etching using so called ion-ion plasmas [22, 23]. This technique is commonly used in the semiconductor industry. In thermonuclear fusion research, H^- sources have been developed to deliver high intensity and high energy beams [24]. After neutralisation by collisional detachment, the beams of neutral hydrogen can be injected into the plasma. This process will be used to heat the fusion plasma at ITER [25].

Negative ions are an important component in the technique of accelerator mass spectrometry (AMS) [26]. The vast majority of accelerators today employ the tandem technique, where negative ions are used in the injection stage. AMS was originally developed to perform sensitive ^{14}C measurements [27]. Today, however, a number of important trace isotopes are studied at these facilities [26]. For example, ^{18}O is an isotope of particular interest, due to its importance in climatology and oceanography [28] research.

There is a large and growing interest in the formation of molecules and their reaction pathways in interstellar space [29]. Positive ions have long been considered important in the formation of large molecules [30]. Since the identification of the first negative ion in an interstellar cloud [31], the interest in negative ions by the astrophysical community has increased significantly.

The main goal of the research presented in this thesis was to increase the understanding of electron-electron correlation by experimental studies of negative ions. In particular, the research focused on investigating very highly excited, and hence highly correlated, doubly excited states. The long term goal of the research project is to investigate doubly excited states in negative ions all the way up to the double detachment limit. These studies necessitated the development of an experimental-system that could be used to measure partial photodetachment cross sections to highly excited final states in the residual atom. Such a system makes it possible to study high-lying doubly excited states in great detail. The technique that was developed in order to investigate partial cross sections is described in this thesis. The method has been applied to the measurement of partial cross sections for photodetachment of K^- and Cs^-. My work also includes a general upgrade of the experimental capabilities at Göteborg University Negative Ion Laser LAboratory, GUNILLA. The mass resolution of the apparatus was improved in order to enable experiments with heavy molecular negative ions. This development was mainly driven by interests in experiments with applications in mass spectrometry [32]. However, the improved mass resolution proved valuable in the experiments on Pt^- and W^- presented in this thesis.

1.1 Basic properties of negative ions

Negative ions differ fundamentally from neutral atoms and positive ions due to the nature of the force that binds the outermost electron. In a neutral atom or positive ion, an electron that is far away from the nucleus experience a Coulomb potential, which scales with distance as $1/r$. In a negative ion, on the other hand, there is no long range interaction between the atom and the outermost electron. The electron is only attracted to the atom by the relatively short range potential that arises from the polarisation of the atom. On a very small scale the binding is best described by electron-electron correlation. At large distances, this interaction asymptotically approaches that of an induced dipole potential, which scales as $1/r^4$. Together with the effective centrifugal potential this gives the radial potential (in atomic units)

$$U(r) = \frac{\ell\,(\ell+1)}{2r^2} - \frac{\alpha}{2r^4}, \tag{1.1}$$

where ℓ is the angular momentum of the electron and α is the static dipole polarisability of the atom. Equation (1.1) cannot be used for small radial distances. The induced dipole model breaks down when the extra electron reaches a radius that is comparable with the size of the occupied orbitals in the neutral atom.

The energy gained when a neutral particle binds an extra electron is commonly known as the Electron Affinity (EA). The EA of an atom is numerically equivalent to the binding energy of the extra electron in the corresponding negative ion. Typically, the EA of an atom is about one order of magnitude smaller than the ionisation potential (IP). In the case of the phosphorus atom, for example, the EA is 0.75 eV while the IP is 10.5 eV [33]. Due to the small binding energies in negative ions the effects of electron-electron correlation are more pronounced than in neutral or positively charged systems. Negative ions are thus ideal test systems for atomic many-body theory.

In atoms or positive ions, the long range Coulomb potential gives rise to infinite series of Rydberg states. Such series are only present in potentials that scales as $1/r$. In contrast, most negative ions have only a single bound state, which might have a number of fine structure components. In this sense, P^- is a typical negative ion, with a single bound term with three fine structure levels. An energy level diagram of P^- is shown in Fig. 1.1. Some negative ions also have different bound terms. An example of this is found in Pt^-, which was investigated in paper **IV**. Bound states with parity opposite to that of the ground state have so far only been identified in Os^- [34, 35] and Ce^- [36].

Optical dipole transitions can only take place between two states of oppo-

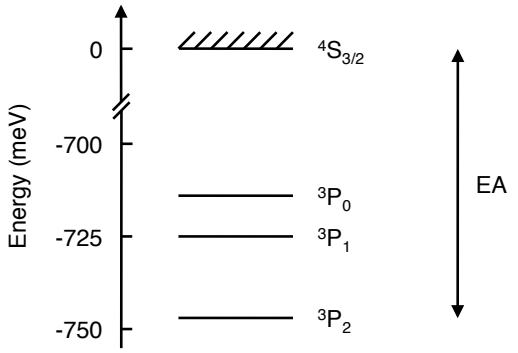

Figure 1.1: *Energy level diagram showing the* ^3P_J *states of* P^- *and the* $^4S_{3/2}$ *ground state of* P. *The spacing of the ion states are to scale. The electron affinity (EA) is indicated as the energy separation between the* $^3P_2$ *ground state of the ion and the ground state of the atom.*

site parity. Therefore, the sophisticated spectroscopic techniques developed to study the structure of neutral atoms cannot, in general, be applied to negative ions since there are essentially no dipole-allowed transitions. Instead of studying bound-bound transitions one must use techniques based on bound-free transitions. For example, when a photon of sufficient energy γ, is absorbed by a negative ion, an electron is ejected in a process called photodetachment

$$P^- + \gamma \rightarrow P + e^-. \tag{1.2}$$

The better known process of photoionisation applies to the ejection of electrons from atoms or positive ions. In solids, the equivalent process is the photoelectric effect.

In photodetachment there are transitions from an initial state of the negative ion to a final state of the residual atom. A particular selection of the initial and final state is often referred to as a channel through which the reaction proceeds. In paper **II**, three photodetachment channels were investigated. In this case the channels were defined by the initial state of the P^- ion. The final state of the residual atom was the same in all channels. The processes studied were transitions from each of the three fine structure components of P^- to the ground state of P. In most cases, however, the channels are defined by the state of the residual atom after photodetachment. In papers **V** and **VI**, for example, the $K^-(4\ ^1S) + \gamma \rightarrow K(5\,^2F) + e^-$ and $K^-(4\ ^1S) + \gamma \rightarrow K(5\,^2G) + e^-$ channels were investigated.

The probability for a photodetachment reaction to take place is described by a cross section (σ_{pd}). Cross sections are expressed in units of area, which illustrates the effective size of the ion. The reaction probability depends on

the photon energy ($\hbar\omega$), and thus $\sigma_{pd} = \sigma_{pd}(\hbar\omega)$. Each photodetachment channel has its specific reaction probability, which is called the partial cross section. In experiments without channel selectivity, the total cross section is measured, which is simply the sum of the partial cross sections for all open channels. When more than one initial state is photodetached, the total cross section depends on the population of these states, and thus the experimental conditions. As such, total cross sections are only of physical significance if the temperature of the ions or the initial state distribution is known. On the other hand, when a single initial state is photodetached to a number of final states, the total cross section has an absolute physical meaning and comparisons between different experiments and calculations can be made.

For optical transitions, there is a well known set of selection rules that describes which transitions that can be induced. Conservation of angular momentum is the most important rule in photodetachment. It is, however, applied in a different way in bound-free transitions than in bound-bound transitions. The detached electron can, namely, acquire any angular momentum necessary so that the total angular momentum change in the reaction is zero. The difference in angular momentum between the states in the negative ion and the neutral is ΔL. In a dipole transition, the photon brings one unit of angular momentum into the reaction. The angular momenta couples vectorially, and thus the detached electron is given an angular momentum of

$$\ell = \Delta\mathrm{L} \pm 1. \tag{1.3}$$

The ± 1 in Eq. (1.3) means that the electron is emitted as two partial waves with different angular momenta. In photodetachment of P^- to the atomic ground state $\Delta\mathrm{L} = 1$, since the transition couples a ^3P states to a ^4S state. The detached electron thus acquires an angular momentum of 0 or 2, i.e., it is represented by a superposition of an s- and a d-wave.

1.1.1 Thresholds

One particularly interesting energy range of a reaction cross section is where the energy is just enough for the process to occur. Each photodetachment channel has its own threshold E_{th}, which is sometimes referred to as a channel opening. Just above threshold, the departing electron has a very low kinetic energy and thus spends a long time close to the residual atom. During this time the outgoing electron interacts with the residual atom and correlations between the electrons develop. These electron-electron correlations influence the shape of the cross section close to the channel opening.

It was shown by Wigner [37], that in the final state of a two-body break-

up reaction, the longest range interaction between the product particles is the one that determines the shape of the cross section at threshold. In the case of photodetachment, the interactions are given by Eq. (1.1). The centrifugal potential is the one that dominates at large distance, due to its stronger radial dependence. The cross section for photodetachment is, according to Wigner [37], given by

$$\sigma_{pd} \propto E_e^{\ell+1/2} = (\hbar\omega - E_{\text{th}})^{\ell+1/2}, \tag{1.4}$$

where E_e and ℓ are the energy and angular momentum of the detached electron, respectively, and $\hbar\omega$ is the photon energy. In general, the outgoing electron is described by two partial waves with different angular momenta, as described above. The higher of the two angular momenta is, however, suppressed close to threshold. As a consequence of this suppression, only s-thresholds ($\ell = 0$) and p-thresholds ($\ell = 1$) are usually observed in experiments. Wigner thresholds with $\ell = 2$ have been observed, but only in two-photon detachment experiments involving circularly polarised light [38].

The Wigner law is strictly only valid at the channel opening. The range of validity above threshold is determined by the finite size of the initial state wavefunction [39] and the strength of other interactions in the system. For example, if the dipole polarisability of the residual atom, second part of Eq. (1.1), is large, the range of validity is reduced. O'Malley [40] has derived an expression based on modified effective range theory (MERT), which includes a correction term to the Wigner law that depends on α. The range of validity of the Wigner law can be estimated by calculating the energy where the correction term becomes larger than a set value (e.g. 5 %). For photodetachment to the ground state of the residual atom, the range of validity of the Wigner law is typically on the order of ten meV [41, 42].

When the polarisability is high, the model by O'Malley cannot be used to describe the threshold behaviour over any significant range [43]. In such cases, more sophisticated models are needed. In an experiment by Sandström *et al.* [43], threshold behaviours involving highly polarisable excited states in alkali atoms were investigated. In that study, a MERT introduced by Watanabe and Green [44] was used to successfully describe the observed thresholds.

1.1.2 Resonances

Atomic negative ions have only a few bound states. Many doubly excited states (DES), however, are embedded in the continuum above the single detachment limit. In the same way as an electron can be bound to an atom

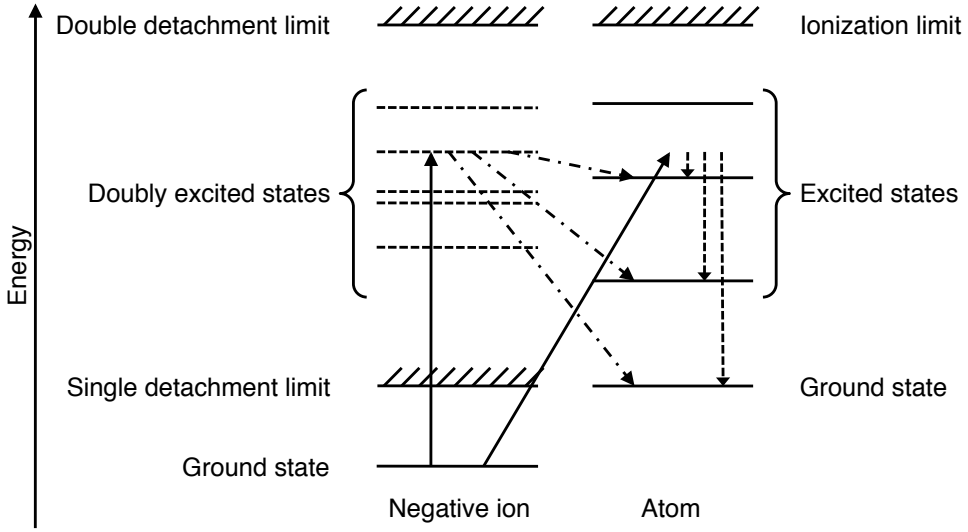

Figure 1.2: *Schematic energy level diagram of a negative ion and the corresponding parent neutral atom. The solid vertical arrow corresponds to an excitation to a doubly excited state. Diagonal dash-dotted arrows represent autodetachment. The oblique solid arrow and the vertical dashed arrows corresponds to the direct photodetachment process.*

in the ground state, an excited atom can also bind an extra electron. Doubly excited states that lie energetically below the parent state are referred to as Feshbach resonances, while DES above the parent state are called shape resonances [45]. Doubly excited states lie in the continuum and, as such, are highly unstable. They preferentially decay via autodetachment to a neutral atom and a free electron on a time scale of picoseconds.

Figure 1.2 shows a schematic energy level diagram of a negative ion and the corresponding neutral atom. A negative ion in the ground state can be promoted to a doubly excited state by the absorption of a single photon (indicated by the solid vertical arrow). The dashed-dotted arrows in the figure represent the autodetaching transition from the DES to bound states in the atom. In the case of a general ion A^-, the whole process can be described as

$$A^- + \gamma \rightarrow A^{-**} \rightarrow A^{(*)} + e^-, \tag{1.5}$$

where A^{-**} is a doubly excited negative ion and $A^{(*)}$ the residual atom, which is possibly excited. The presence of the doubly excited states introduce modulations in the photodetachment cross section. The structures are known as resonances. In the case of a shape resonance that decays to the parent state, the cross section modulation takes the form of a pure enhancement with

the shape of a Lorenz profile. When, on the other hand, the decay leads to a state below the parent state, there are two paths that leads from A^- to $A^{(*)}$. The direct, non-resonant, path is described by the oblique solid arrow and the dashed arrows in Fig. 1.2. The resonant path is described above. These two competing paths lead to quantum interference, which can either enhance or reduce the cross section compared to the non-resonant photodetachment cross section. Resonance structures can have different shapes due to different intrinsic phase shift between the two paths. One way of describing cross section modulations due to a resonance is by a Shore profile [46]

$$S = \frac{a\epsilon + b}{\epsilon^2 + 1}, \tag{1.6}$$

where a and b are the so called Shore parameters and $\epsilon = (\hbar\omega - E_\mathrm{r})/\frac{\Gamma}{2}$ is a scaled dimensionless energy parameter. The resonance energy, E_r, and the resonance width, Γ, are used in the scaling. The modulation of a cross section due to a resonance can be described by multiplying the expression in Eq. (1.6) with a function describing the non-resonant cross section [47].

1.2 Experimental perspective

Many different experimental techniques have been employed in studies of properties of negative ions. In the experiments presented in this thesis, laser photodetachment has been used. In principle, one can study either the free electron or the residual atom that are produced in the final state of a photodetachment reaction. In this thesis, photodetachment cross sections were measured by recording the number of neutral atoms produced as a function of photon energy. Negative ion binding energies can be determined by fitting the Wigner law to cross section data in the corresponding threshold regions. In the literature, this method is referred to as Laser Photodetachment Threshold Spectroscopy (LPTS).

An alternative method, Photoelectron Spectroscopy (PES), is based on measurement of the energy of the detached electron. In this case, a fixed frequency laser is used to photodetach the electron. Photodetachment microscopy is a special version of PES for negative ions, which was developed by Blondel *et al.* [48]. In this method, the photodetachment process takes place in a homogeneous electric field, which projects the electrons onto a position sensitive detector. Each point on the detector can be reached by two possible trajectories. The wavefunctions for the two paths interfere and the interference pattern is used to determine the energy of the electrons. The high resolution inherent in the interferometric measurement has resulted in the

determination of electron affinities in some elements [49] with unprecedented precision. Another method, which should not be confused with photodetachment microscopy, is Velocity Map Imaging (VMI). Like photodetachment microscopy, VMI is based on projecting the photoelectrons onto a screen using an electric field. Instead of using an interferometric measurement, however, the energies are determined directly by the size of the electron distribution on the screen. The angular distribution of the photoelectrons with respect to the laser polarisation can be directly imaged using the VMI technique [50].

In early experiments designed to study the high-lying doubly excited states of H^-, Harris *et al.* [6] took advantage of the Doppler shift and used it to tune the photon energy. In that work, a relativistic H^- beam was intersected by the fourth harmonic of a Nd:YAG laser. By varying the angle between the two beams [51], photon energies in the ion frame up to 14 eV could be achieved. Direct electric field ionisation of the final $n = 4 - 7$ states in H, was used to measure partial cross sections. The same detection method was used by Petrunin *et al.* [11] in a measurement of partial cross sections in He^- photodetachment to the $n = 11 - 14$ states.

The direct field ionisation technique gives access to highly excited final states, but suffers from a low specificity in the final state detection. No selectivity in the angular momentum of the detected states is, for example, achieved. Moreover, when the photon energy is tuned above the opening of the next detachment channel, a sum of partial cross sections is measured. Full selectivity in the final state detection can, however, be achieved by the use of a resonance ionisation scheme [52]. Such a method was used to perform the partial cross section measurements presented in this thesis.

Doubly excited states in negative ions can also be studied by investigating the scattering of electrons on neural atoms. An incident electron can then be temporarily captured into a doubly excited state before it is re-emitted. The presence of resonant states are then observed as modulations in the scattering cross section [53].

Electrons are also used to directly detach electrons in collisions with negative ions. With this technique, it is possible to study single and multiple collisional detachment from negative ions [54, 55]. Resonance structures have been observed in electron collision experiments with diatomic and polyatomic molecular negative ions. These resonances have been attributed to the formation of excited doubly charged negative ions [56, 57]. Such resonances were believed to exist also in atomic negative ions. The existence of H^{2-} was considered a possibility at one time [58, 59]. Later experiments, however, disproved the possibility [60]. Most of the electron impact studies of negative ions have been performed in magnetic storage rings, such as CRYRING in Stockholm [56] or ASTRID in Aarhus [57], which were dedicated to atomic

and molecular physics. In recent years, however, electrostatic storage rings have been constructed. This innovation makes it possible to study heavier molecular negative ions [61]. Electrostatic and [62] radio frequency [63] traps have also emerged as important tools for studies of negative ions.

Some photodetachment experiments on atomic negative ions have been performed at synchrotron light sources. The high energy UV and X-ray photons available at such facilities makes it possible, for example, to study core electron detachment. Since the energy supplied by these photons is well above the double detachment limit, the photodetachment of a core electron is followed by Auger decay, which leads to the production of a positive ion that can be detected. Resonances attributed to core-excited states of negative ions are often seen in this kind of experiments [64, 65].

Most of the discussion so far has focused on atomic negative ions. Studies of molecular and cluster negative ions are, however, becoming increasingly important. This is especially true in astrophysics after the first negative ion, C_6H^-, was detected in an interstellar cloud by McCarthy *et al.* [31]. The structure of molecular ions is much more complex than atomic negative ions due to the additional degrees of freedom. The large number of rotationally , vibrationally and even electronically excited states make the analysis of photodetachment spectra much more complicated [66, 67].

CHAPTER 2

Experimental method

The experiments presented in this thesis have been performed using an ion beam apparatus situated at Göteborg University Negative Ion Laser LAboratory, GUNILLA. A schematic of the apparatus is shown in Fig. 2.1. At this facility, a negative ion beam was extracted from a Caesium sputter source. After mass selection in a magnet the beam was deflected into an interaction region. In the interaction region, a laser beam was overlapped with the negative ion beam in a collinear geometry. Free electrons and neutral atoms were produced by photodetachment of the negative ions. Cross sections for such processes were measured by counting the number of atoms produced as a function of the energy of the photons from the laser.

2.1 Ion beam apparatus

The ion beam apparatus at GUNILLA has been upgraded as a part of this thesis work. The mass resolution of the apparatus was improved in order to enable measurements on heavy molecular ions, primarily motivated by applications in mass spectrometry [32]. The full description of the ion beam apparatus is given in paper **I**. Only a summary is given in this chapter.

The apparatus was designed to allow the laser and ion beams to interact in a merged beams geometry. One of the major advantages of the merged beams technique is that the interaction volume can be up to a hundred times larger than that obtained using crossed beams. It is, however, more difficult to ensure a homogeneous and constant overlap between the two superimposed

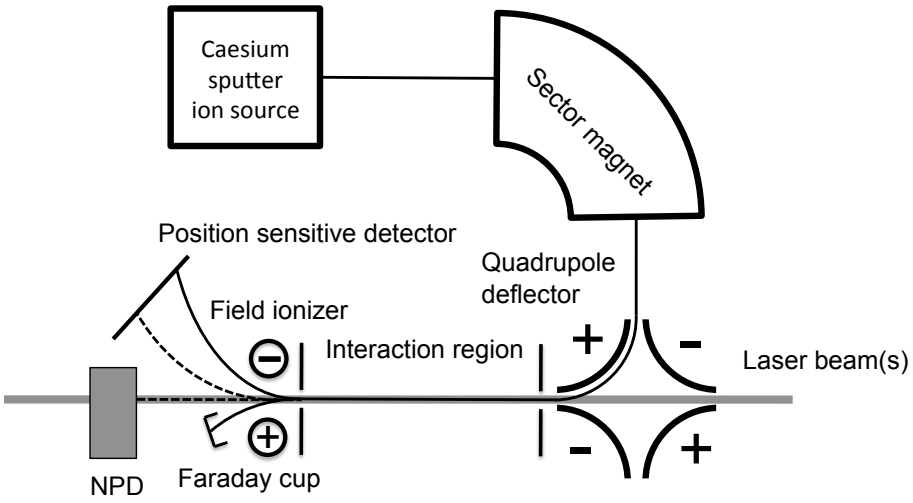

Figure 2.1: *A sketch of the experimental set-up. Both the neutral particle detector (NPD), and the position sensitive detector are shown. Only one at the time was mounted during experiments.*

beams. At GUNILLA, this problem is handled by defining an interaction region using two 3 mm diameter apertures placed 61 cm apart. A good overlap is ensured by optimising the transmission of both the ion- and the laser-beam through the interaction region.

The phase space volume occupied by an ion beam is given by the positions and angles of the beam particles relative to the center axis. This quantity is known as emittance and according to Liouvilles theorem it cannot be changed by conservative fields. Acceptance is a corresponding quantity that indicates the maximum phase space volume that can pass through an ion optical component. The acceptance of the interaction region in the present apparatus is 3.7 π mm mrad, while the emittance of the beam leaving the ion source is approximately 50 π mm mrad. The maximum transmission through the apparatus is thus $(3.7/50)^2 \approx 0.5$ %. In order to achieve the optimal transmission, however, the ion beam has to be directed and focused to match the acceptance of the interaction region.

Negative ions are produced in a caesium sputter source and are accelerated to and energy of 6 keV. A sputter source is versatile and can produce negative ions of most elements. It is also reliable and rather easy to operate. The main drawbacks with a sputter source are the wide energy distribution of the ions leaving the source and the high emittance of the produced ion

beam. Furthermore, ions with small electron affinities are often produced only in small quantities.

A sector magnet is used as the mass dispersive element in the apparatus. An object slit placed in front of the magnet and an image slit placed after the magnet ensure that only a single mass can be transmitted through the apparatus. The magnet is single focusing and affects only the focal properties of the beam in the horizontal plane. An ion optical system based on two single-focusing lenses produces a symmetric beam after the magnet. This makes it possible to match the ion beam with the cylindrical interaction region and hence optimise the transmission through the system. An Einzel lens and a single focusing lens, with horizontal focusing, are placed in front of the object slit. A second single focusing lens, with vertical focusing, is placed between the magnet and the image slit. With this combination it is possible to focus the beam in both the horizontal and vertical directions at the position of the image slit.

Three Faraday cups are used to monitor the ion beam current before and after the interaction region. A cup placed in the end of the beam path, shown in Fig. 2.1, is used to measure the ion current during experiments. The other two cups are retractable and are placed after the object and image slits, respectively. The Faraday cups behind the slits are used to ensure that the ion beam foci are correctly positioned during the alignment of the beam.

The measured transmission is, as described in paper **I**, close to the theoretical limitation of 0.5 %, given by the ratio of the acceptance of the interaction region and the emittance of the ion source. The mass resolution was characterised by studying mass spectra of W^- and $WF_5{}^-$. The mass resolution for molecular ions, measured after the image slit was, in agreement with the theoretical value of $M/\Delta M = 500$. In the case of atomic ions the kinetic energy distribution of the ions was wide, which lowered the measured mass resolution to 350. Using the Faraday cup placed after the interaction region, however, the mass resolutions were found to be 500 and 800 for atomic and molecular ions, respectively. This increase in the mass resolution is not yet completely understood. Most likely, it is caused by the interaction region acting as an effective aperture that is smaller than the image slit.

2.2 Measurements

The photodetachment process, as described by Eq. (1.2), results in a free electron and a neutral atom. The number of photodetachment reactions,

n_{pd}, per laser pulse is given by

$$n_{\mathrm{pd}} = \frac{\sigma_{\mathrm{pd}} N_{\mathrm{ion}} N_{\gamma}}{A}, \tag{2.1}$$

where σ_{pd} is the cross section for photodetachment, A is the cross sectional area of the interaction region, and N_{ion} and N_{γ} are the number of ions in the interaction region and the number of photons in the laser pulse, respectively. The cross section for the reaction can be measured by counting either the emitted electrons or the residual atoms. The electrons are ejected from the individual ions of the beam all along the length of the interaction region. The residual atoms, however, continue in the forward direction due to their larger mass. In a merged beams experiment, the photoelectron emission pattern makes it very hard to efficiently collect and detect the electrons [68]. The neutral atoms, on the other hand, can be easily detected due to their well defined trajectories and large energies. These residual atoms can, for example, be counted by a channel electron multiplier (CEM) or a microchannel plate (MCP). Both devices give a measurable current pulse following the impact of just a single particle. This type of detector was used in the measurements of total cross sections that are described in papers **II**, **III** and **IV**. However, in order to measure partial photodetachment cross sections, as described in papers **V**, **VI** and **VII**, one has to incorporate a state-selective detection scheme. These two types of detectors are both shown in Fig. 2.1 and are described in the two following sections.

Two different OPOs (optical parametric oscillator) have been used as light sources in the experiments presented in this thesis. They are both pumped by nanosecond Nd:YAG lasers with 10 Hz repetition rate. The systems are based on the non-linear effect of parametric conversion and can produce radiation with wavelengths in the ranges 220-1800 nm and 1350-5000 nm, corresponding to photon energies of 0.69-5.6 eV and 0.25-0.92 eV, respectively. OPOs are relatively easy to use but have an inherent instability from shot to shot that increases the effective bandwidth. As discussed in paper **II**, the specified bandwidth of the lasers are 0.2 cm^{-1} ($\approx 0.25\mu$eV), while the difference in the central photon energy from shot to shot can be more than an order of magnitude larger. This problem has been solved, as described in paper **II**, by measuring the wavelength of each laser shot. A commercial wavelength meter is used for this purpose. The wavelength of each pulse is stored together with measured values of all other relevant experimental parameters.

After an experiment the data is sorted and binned based on the measured wavelength. Photodetachment cross sections are then calculated using the

expression

$$\sigma_i = \frac{n_i \, \hbar\omega_i}{I_i \, E_i}, \tag{2.2}$$

where σ_i is the cross section calculated for a bin with photon energy $\hbar\omega_i$, n_i is the mean number of counts per laser pulse in the bin, and E_i and I_i are the mean pulse energy and ion current, respectively.

Photon energies are measured in the laboratory reference frame, but it is the photon energy in the rest frame of the ion that is relevant in the photodetachment process. The Doppler shift can be calculated from the acceleration voltage and the mass of the ion, and thus the measured photon energy can be corrected for the motion of the ions. This correction adds to the uncertainty in the energy scale on the order of 20 μeV, depending on the ion mass. The major contribution to the uncertainty in the Doppler correction arises from the uncertainty in the ion beam energy. However, the Doppler shift in a measured threshold energy can be eliminated without knowledge about the ion beam velocity. This is achieved by determining the threshold energy with the laser beam both co- and counter propagating with the ion beam. The Doppler shift is then corrected in all orders by taking the geometric mean of the blue- and red-shifted threshold energies [69]. This method was used in the measurement presented in paper **II**.

It is, in principle, possible to extract absolute photodetachment cross section from the measurements by use of Eq. (2.2). However, the geometrical overlap factor between the beams and the efficiency of the detector have to be incorporated in the expression. In a crossed beams experiment, the overlap factor can be eliminated by translating one beam through the other. This method has been shown to work with both electron beams [70] and laser beams [71]. The degree of overlap in a collinear beams experiment can be deduced if the cross sections of the beams are measured. This was for example achieved in the work by Covington *et al.* [72] end Bruhns *et al.* [73], where beam scanners were placed in the interaction region. The ion beam apparatus in GUNILLA is not equipped with such devices, and hence only relative cross sections are presented.

The velocity spread of the ions produced in the ion source is compressed since all ions are accelerated over the same electrical potential. The reduced width of the velocity distribution produces a reduced Doppler broadening which in experiments with a collinear interaction geometry. This enhances the spectroscopic resolution of the measurements [74].

2.2.1 Neutral detection

Total cross sections were measured by counting the number of neutral atoms that were produced by photodetachment in the interaction of the laser and ion beams (papers **II**, **III** and **IV**). The first step in the detection of the residual neutral particles is to separate them from the negative ion beam. This is achieved by deflecting the negative ions with an electrical field after the interaction region (see Fig. 2.1). Neutral particles are unaffected by the field and continue straight forward to a particle detector. The laser pulse energy must be measured for normalisation purposes as can be seen in Eq. (2.2). The obvious way to measure the amount of radiation that interacts with the ion beam is to detect it after the interaction region. This, however, requires that the detector is transparent to the laser radiation since the neutral particles and the radiation follow the same path.

In the neutral particle detector, the residual atoms impinge on a glass plate with a conductive coating. The coating is made of tin-doped indium oxide, which is transparent in the visible region and into the near IR and UV regions [75]. The transmission window of the glass plate is, however, smaller than the full photon energy range of the lasers available at GUNILLA. When a heavy particle with a kinetic energy in the keV region strikes the glass plate, secondary electrons are emitted. These electrons are accelerated towards the front of a CEM, in which a measurable current pulse is produced. The conductive coating on the glass plate prevents it from becoming electrically charged. The signal from the CEM is decoupled from the high voltage using a capacitor situated outside the vacuum chamber. The current pulses are converted to voltage pulses using a fast amplifier. In papers **II**, **III** and **IV**, these pulses were counted for each laser shot using a gated counter, that was triggered by the laser pulse.

Only a single particle can be detected per laser pulse in crossed beams experiments employing pulsed lasers and particle counting. In this case, the interaction region is so small that two particles, created by the same laser pulse, would arrive at the detector so close in time that they would be indistinguishable. To avoid detector saturation, the maximum count rate that can be allowed in such an experiment is on the order of 0.1 per laser pulse. With collinear beams, on the other hand, the neutrals that are produced are spatially distributed over the whole interaction region. The flight time of these particles from the interaction region to the detector is sufficiently large to allow multiple particles to be detected for each laser pulse. The maximum number of counts per laser pulse is then determined by the recovery time of the detector. The CEM used in our experiments requires 0.1-1 μs to recharge and become ready for the detection of the next particle. Detector saturation

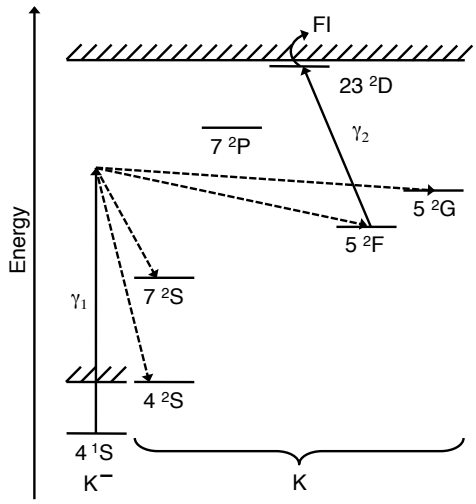

Figure 2.2: *Partial energy level diagram of* K^-*, showing the resonance ionisation scheme.* γ_1 *photodetaches the ion, populating all available states.* γ_2 *is used for detection. The excitation of the* $5\,^2F$ *state to the Rydberg state* $23\,^2D$ *is illustrated. The Rydberg state is field ionised (FI) and the produced* K^+ *is detected.*

was avoided by keeping the count rates at less than one per microsecond.

2.2.2 State selective detection

The state-selective detection scheme implemented at GUNILLA is based on resonance ionisation of the residual atoms produced by the photodetachment process [52]. Figure 2.2 shows a partial energy level diagram of the K^- and K systems. It also illustrates the resonance ionisation scheme used in the experiments.

Photodetachment is performed with laser γ_1. Following the detachment of an electron, the residual atoms is left in a wide distribution of excited states. The final state channel is defined by the excited state of the residual atom. The reactions

$$\begin{aligned} K^- + \gamma_1 \rightarrow \quad & K(7\,^2S) + e^-, && (2.3)\\ \rightarrow \quad & K(5\,^2F) + e^-, && (2.4)\\ \rightarrow \quad & K(5\,^2G) + e^-, && (2.5) \end{aligned}$$

are the channels investigated in papers **V** and **VI**. In order to achieve final state selectivity, a second laser (γ_2) is used to resonantly excite from one of

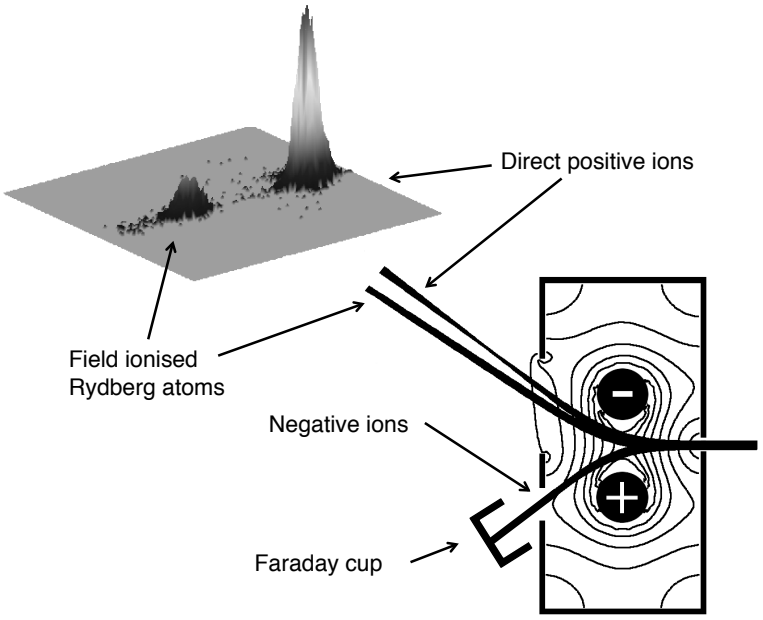

Figure 2.3: *Field ioniser with contours showing lines of equal field strength. Ions enter from the right. Field ionised Rydberg atoms are deflect less than the positive ions. Two clearly separated peaks are seen on the detector.*

the final states of the residual atom to a Rydberg state, for example

$$\mathrm{K}(5\,^2F) + \gamma_2 \rightarrow \mathrm{K}(23\,^2D), \tag{2.6}$$

as shown in Fig. 2.2.

The beam from the second laser was selected to be co-propagating with the first laser beam and the ion beam. Rydberg atoms produced by the second laser are efficiently ionised in a relatively weak inhomogeneous electric field and the produced positive ions are detected. Figure 2.3 shows how the field is created by two cylindrical electrodes. When the beam particles enter the field, negative and positive are deflected in opposite directions. Neutral Rydberg atoms, on the other hand, travel straight forward until the field strength becomes sufficiently strong for ionisation to occur. Positive ions created by field ionisation are then deflected, but they follow a different trajectory than those particles that enters the field as positive ions. A position sensitive detector (PSD) is used to detect and distinguish between positive ions created in the field ionisation of Rydberg atoms and those that have been created in the interaction region. This is illustrated in Fig. 2.3. The spatial separation of the positive ions of different origins enhances the signal-to-background ratio since a potentially large background can be avoided.

The photon energy of the photodetaching laser, γ_1 in Fig. 2.2, is larger than the ionisation potential of the atom. Hence, many positive ions are created in the interaction region via the sequential two photon photodetachment-photoionisation process. The detector image in Fig. 2.3 indicates that the direct positive ion peak is larger than the peak arising from the field ionised Rydberg atoms. This image is, however, not recorded with the high photon energies used in papers **V**, **VI** and **VII**. In the experiments described in this thesis, the direct peak was approximately 100 times larger than the peak that arose from the field ionised Rydberg atoms. The latter peak constituted the signal in the experiments.

The detector is based on an MCP stack. Two delay line wires are placed behind the MCP stack to collect the electrons produced in the cascade initiated by the impact of a heavy particle. The deposition of charge on the wires create electrical pulses that propagate towards the ends of the wires. By measuring the time difference between the arrival of the pulses at the ends of the wires, it is possible to extract information about the position of the impinging particle on the face of the detector. The times of arrival of the electrical pulses are measured to a 25 ps accuracy by use of a time-to-digital converter (TDC).

The position sensitive detector is circular and has an active area with a diameter of 40 mm and a spatial resolution that is better than 0.1 mm. The detector is able to handle count rates up to 1 MHz. When multiple hits occur, it has a dead time of 10-20ns. In order to reduce problems caused by high count rates, the experiments were performed with the direct positive ions deflected just outside the active area of the detector.

Unfortunately, the energy of the UV photons used to photodetach the negative ions (γ_1), is sufficiently high to be detected by the MCP. The number of photons in a laser pulse is so large, that the MCP is completely saturated even if only a small fraction of the photons are scattered towards the detector. The saturation is so severe that it is not possible to detect particles within tenths of microseconds after the laser pulse. This time span includes the full range of arrival times of particles travelling from the interaction region. This serious problem is avoided by switching the electrical potential on the front of the MCP stack using a timing cycle based on the laser pulse and the arrival of the signal. The voltage across the MCP stack is lowered before the laser pulse strikes, thus reducing the gain of the detector. It is then increased again before the positive ions from the interaction region arrives at the detector. In the off mode, the MCP is run with +2.2 kV applied to the back, while the front voltage is +0.8 kV. Right after the laser pulse, a transistor grounds the front of the MCP stack, thus activating the detector. The switching takes less than 0.5 μs, but a ringing is induced on the delay

lines that lasts up to 1.2 μs.

For each laser pulse, the ion beam current, the laser pulse energy and the laser wavelength are measured and stored, as in the experiments with the neutral particle detector. However, instead of storing the number of hits for each laser shot, all the timing information from the TDC is recorded. After a completed scan, the detector data is analysed and the information on the positions of the hits is extracted from the delay line times. Since no time gates or spatial cuts are set in the measurement, optimised cuts can be determined in the off-line analysis. With the created cuts in the detector data, cross sections are calculated in the same way as in the experiments with the neutral particle detector, using Eq. (2.2).

CHAPTER 3

Results and discussion

This chapter summarises the results presented in the papers **II** to **VII**. The first three papers treat the bound state structure of P^-, W^- and Pt^-. These experiments involve measurements of total photodetachment cross sections using neutral particle detection. The last three papers, describing experiments on K^- and Cs^-, are based on measurements of partial photodetachment cross sections.

3.1 Phosphorus

The energy level diagram of P^- is shown in Fig. 1.1. In the investigation of P^-, the electron affinity and the fine structure intervals of the three bound ^3P_J (J = 0, 1, 2) states were measured. These quantities have previously been determined [76, 77] using LPTS in studies similar to the present experiment. The aim of the experiment described in paper **II** was to improve the accuracy of the experimental values.

Figure 3.1 shows the three photodetachment thresholds resulting from detachment of the P^- ion in the three different ^3P_J fine structure levels. A detailed scan over the threshold for the $P^-(^3P_0)$ channel is shown in the insert. Photodetachment from a ^3P_J state in P^- to the $^4S_{3/2}$ state in P results in an electron leaving as an s-wave. The threshold energies were extracted by fitting the Wigner law, Eq. (1.4), with $\ell = 0$ to the data. The range of validity of the Wigner law was estimated to be at least 5 meV in all the three thresholds.

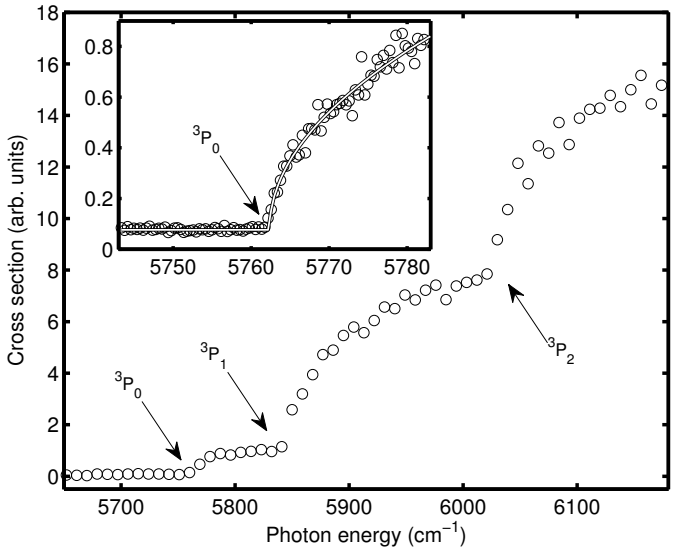

Figure 3.1: *Cross section for photodetachment from* P^-*. The three thresholds corresponds to the fine structure components of the bound* ^3P_J *term. The insert shows the lowest threshold in more detail. It also contains a fit of the Wigner law (Eq. 1.4) with* $\ell = 0$*. The data was recorded with counter propagating laser and ion beams, and the data is thus blue-shifted.*

The factors contributing to the uncertainty in the threshold energies were the finite laser bandwidth and the background signal from the fine-structure channels with smaller binding energies. The background is very small below the lowest energy threshold which corresponds to the ion being in the $^3P_0$ state prior to photodetachment. The background in this case originates in collisional detachment only. The uncertainty in the energy of this threshold was therefore the smallest. The Doppler shift correction in the case of the $^3P_0$ threshold was performed by calculating the geometric mean of the threshold energies for co- and counter-propagating laser and ion beams. The Doppler shifts for the higher energy thresholds were calculated from the known acceleration voltage.

These experiments yielded values of the EA of P and the fine structure splittings in the P^- ion. The results are summarised in Table 3.1. The table also gives the values from the previous measurements [76, 77] and a recent calculation by de Oliveira *et al.* [78]. There is a remarkable agreement between the present determination of the EA and the value from the *ab initio* calculation performed using density function theory.

Table 3.1: *The fine structure intervals in* P^- *and the EA of* P. *The experimental values of Feldman [76] and Slater and Lineberger [77] and the EA calculated by de Oliveira et al. [78] are given for comparison. The recommended values by Andersen et al. [20] are also shown.*

$J - J'$	2-0	2-1	1-0	EA
Feldman	-	22.46	10.16	746.76(50)
Slater	32.6(4)	22.4(4)	-	746.4(4)
Andersen	32.6(3)	22.4(3)	-	746.5(3)
de Oliveira	-	-	-	746.7
Present data	32.73(7)	22.48(7)	10.25(3)	746.68(6)

3.2 Platinum

The structure of Pt^- was not fully known prior to the measurement presented in paper **IV**. The present measurement of the binding energy of the $^2S_{1/2}$ state, however, has resolved the problem. The binding energies of the $^2D_{5/2}$ ground state and the excited $^2D_{3/2}$ state had previously been measured to be 2.125 10(5) eV [79] and 917.4(1) meV [80], respectively. Thøgersen *et al.* have also calculated the binding energy of the $^2D_{3/2}$ state to be 943 meV [80], while a calculation by Zollweg indicated a binding energy of 915 meV [81]. Zollweg and Thøgersen *et al.* have also performed calculations for the $^2S_{1/2}$ state, resulting in binding energies of 532 meV [81] and 724 meV [80], respectively. Figure 3.2 shows an energy level diagram (to scale) of the Pt^- states and the lowest states in Pt. The theoretical predictions and the measured value for the energy of the $^2S_{1/2}$ state are given in the figure.

The calculations indicated that $^2S_{1/2}$ was the least bound state in the ion. Therefore, the experiment started with probing from the detachment threshold for the $^2D_{3/2}$ state. Photodetachment signal was observed below this threshold, so the conclusion was drawn that theory was correct about the ordering of the states. The detachment threshold for the $^2S_{1/2}$ state was then located by tuning the laser to smaller photon energies.

The photodetached electron leaves the atom as a combination of partial p- and f-waves. The higher angular momentum component, $\ell = 3$, is suppressed by the centrifugal barrier so a Wigner threshold law with $\ell = 1$ was successfully used to fit to the data. The resulting threshold energy, after taking the Doppler shift into account, was 849(2) meV.

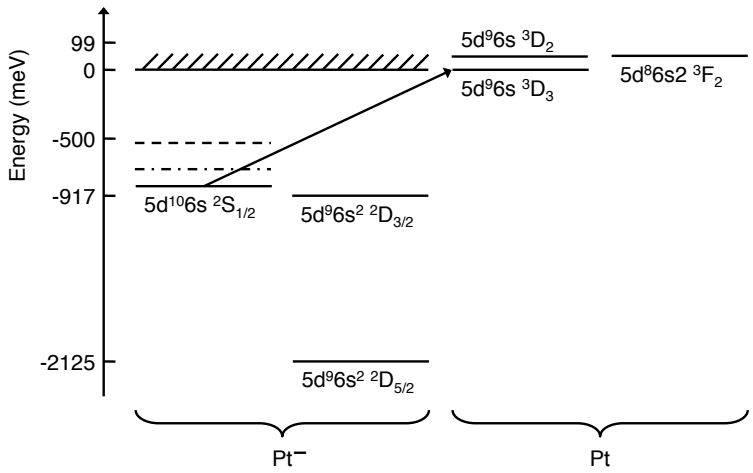

Figure 3.2: *Energy levels in* Pt^- *and the lowest levels in* Pt. *The arrow indicate the transition investigated in the experiment. The predictions for the position of the* $^2S_{1/2}$ *state by Zollweg [81] and Thøgersen et al. [80] are indicated by a dashed and a dash-dotted lines, respectively.*

3.3 Tungsten

The best previous measurement of the electron affinity of the W atom was a PES measurement by Bengali *et al.* [82]. This yielded a value of 817(4) meV. The goal of the experiment presented in paper **III** was to reduce the uncertainty in the EA value. The threshold energy was well known, so the experiment was performed by simply tuning the photon energy across the threshold region. In total, 18 scans were recorded. The sum of these scan is shown in Fig. 3.3. The threshold energy was extracted by fitting the Wigner law, Eq. (1.4), with $\ell = 1$ and the value was corrected for the Doppler shift, which was calculated using the known acceleration voltage. This procedure produced an experimental value for the EA of W of 816.26(8) meV, in good agreement with the previous measurement of Bengali *et al.* [82]. The uncertainty in the present value has been, however, reduced by a factor of 50 over the previous measurement.

In Fig. 3.3, a rather large signal is observed below the threshold, even though the collisional background has already been subtracted. A number of different tests were performed to understand the origin of this background. The mass spectrum showed a clean fingerprint of the natural abundances of the W isotopes. However, even very small amounts of a contaminant, such as, WH^- or WH_2^- ions could be the source of the signal below the threshold if the relevant photodetachment cross section is sufficiently large.

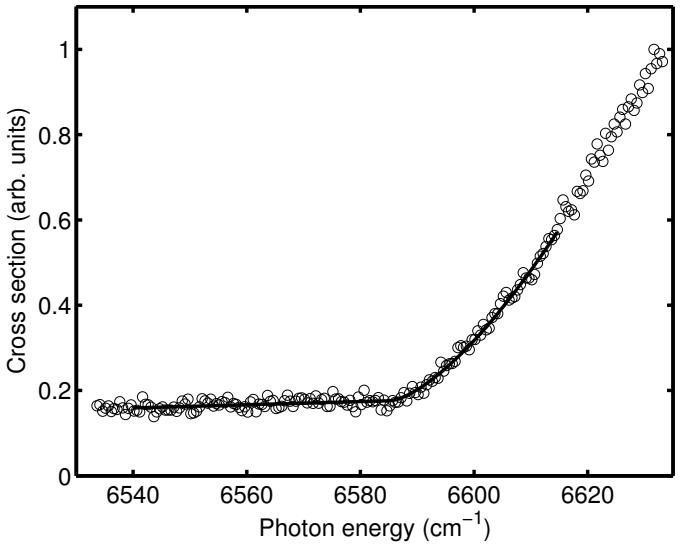

Figure 3.3: *Threshold for photodetachment of the ground state* W^- *ion. The relative cross section data consists of the sum of 18 separate scans. The solid line represents a fit of the Wigner law to the data.*

To investigate this possibility, the photodetachment signal was recorded as a function of the mass of the ions in the beam, using a photon energy of 805 meV. This photon energy is well below the threshold for detachment of ground state W^-. An analysis of the mass spectrum indicated that the mass peak at 182 was almost pure W^-, with the fraction of hydrides being estimated at less than 10^{-5}. We were therefore able to conclude that the signal below the detachment threshold seen in Fig. 3.3 most likely arises from photodetachment of W^- in a previously unknown excited state. Attempts were made to search for the photodetachment threshold for this state by tuning the laser to smaller photon energies. The vacuum windows and the detector glass plate did, however, set a limit on the tuning range in the infrared wavelength region. The threshold was not located using the available tuning range. The photodetachment signal was, however, still observed at photon energies of 385 meV. This observation gives an upper bound on the binding energy of the new state[1].

[1] Rohlén *et al.*, have recently demonstrated that excited state in question has a binding energy that is smaller than 250 meV. This unpublished study, which is not part of the present thesis, was performed using a crossed beams geometry.

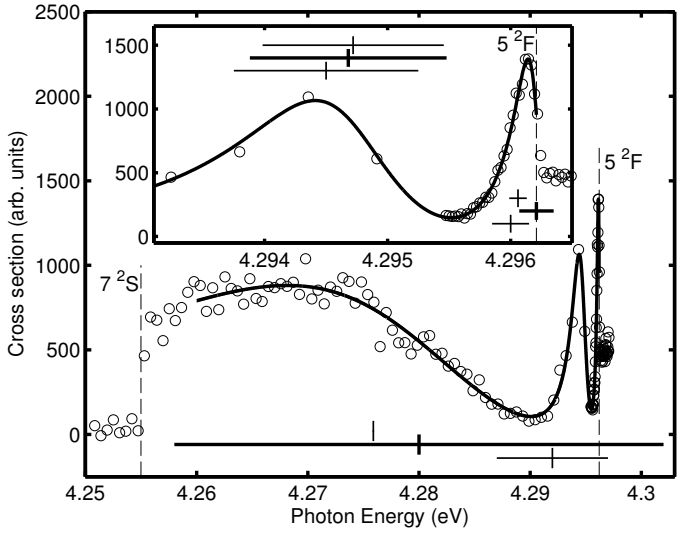

Figure 3.4: *Partial cross section for photodetachment of* K^- *into the* $K(7\,^2S)$ *channel. The solid line is a fit of Eq. (3.1). Resonance energies and widths are indicated by the vertical and horizontal lines, respectively. The resonance parameters from the current experiment are given with thick lines, thin lines represent values from Liu [83] and Kiyan et al. [10], above and below the thick lines, respectively. Liu did not quote a width for the resonance at 4.28 eV. Vertical dashed lines mark channel openings.*

3.4 Potassium

Kiyan *et al.* [10] studied the partial cross section for photodetachment from K^- to the $5\,^2S$ state in K. Their measurement covered the 4.193 – 4.298 eV photon energy range extending just above the $K(5\,^2G)$ threshold. In a subsequent paper, Liu [83] presented theoretical cross section curves and resonance parameters up to 4.36 eV, which is above the $K(7\,^2P)$ channel opening. Partial cross sections were, however, only given up to energies of 4.26 eV except in the $K(5\,^2S)$ channel.

In the experiment described in paper **V**, photodetachment to the $7\,^2S$, $5\,^2F$ and $5\,^2G$ states in the residual K atom were investigated (Eqs. (2.3), (2.4) and (2.5)). The photon energy range extended from 4.250 eV to 4.360 eV, which encompasses energies from below the $K(7\,^2S)$ threshold to above the $K(7\,^2P)$ channel opening.

In the region below the $K(5\,^2F)$ threshold, shown in Fig. 3.4, three resonances were observed in the $K(7\,^2S)$ channel. An expression involving three

Shore profiles [46] and a linear background [47]

$$\sigma = (c + \hbar\omega\, d)\left(1 + \sum_{i=1}^{3} S_i\right) \tag{3.1}$$

was used as used to fit to the experimental data in order to extract the energies and widths of the resonances. In Eq. (3.1), c and d are constants describing the non-resonant cross section, $\hbar\omega$ is the photon energy and S_i a Shore profile, is defined by Eq. (1.6). Figure 3.4 includes a fit to the data, shown as a solid line. The resonance energies and widths are indicated by the vertical and horizontal lines respectively. The figure also shows the resonance parameters from Liu [83] and Kiyan *et al.* [10]. The numerical values of these parameters are compiled in Table 3.2. The table also includes a fourth, very narrow, resonance, that was observed by Kiyan *et al.* and Liu. This resonance was, however, not observed in the present measurement. A comparison of the present cross section for the K($7\,^2S$) channel and the cross section for the K($5\,^2S$) channel investigated by Kiyan *et al.* illustrates an interesting and important fact. Resonance modulation of a non-resonant partial cross section increases as the level of excitation of the residual atom increases. In the present measurement, it is as high as 90 % but in the same energy region it only reaches 25 % in the measurement of Kiyan *et al.* [10].

No previous experimental studies have been performed in the energy region between the K($5\,^2F$) and the K($7\,^2P$) channel openings. The calculation by Liu [83], however, predicts the shape of the total photodetachment cross section in this energy region. He also quotes parameters for the two resonances that were predicted. Three partial cross sections were measured in this energy region and all of them are shown in Fig. 3.5. Two resonances are visible in the cross sections, in agreement with the calculation by Liu. The most interesting feature is, however, the difference in threshold behaviour in the K($5\,^2F$) and K($5\,^2G$) channels. The different threshold behaviours were investigated and the results were published in paper **VI**. They are discussed in section 3.4.1. The threshold model

$$\sigma_{\mathrm{th}} \propto \exp\left(DE_e^{1/4}\right), \tag{3.2}$$

developed to describe the non-resonant cross section in the K($5\,^2G$) channel also represents the background in the analysis of the resonant structure. In Eq. (3.2), D is a numerical constant that is used as a free parameter in the fit.

Resonance parameters were extracted by fitting the two-resonance form of Eq. (3.1) to the data in the K($7\,^2S$) and K($5\,^2F$) channels. In the fit to the

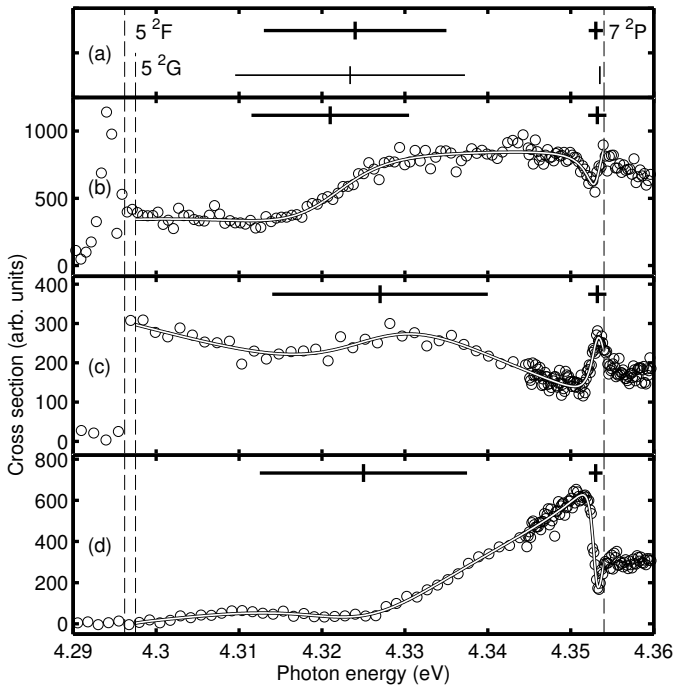

Figure 3.5: *Partial photodetachment cross sections for* K^-*. Panels (b), (c) and (d) show the* $K(7\,^2S)$*,* $K(5\,^2F)$ *and* $K(5\,^2G)$ *channels, respectively. Fits of Eq. (3.1) are shown as hollow lines. Resonances parameters are indicated with the thick vertical and horizontal lines in the corresponding panel. The thick lines in panel (a) are the weighted means of the resonance parameters. The resonance parameters calculated by Liu [83] are indicated by the corresponding thin lines (no width given for resonance at 4.353 eV). Dashed lined indicate channel openings.*

$K(5\,^2G)$ data, the threshold law in Eq. (3.2) was used to represent the non-resonant cross section instead of the linear function in Eq. (3.1). The fits to the data are shown together with the resonance parameters in Fig. 3.5. The resonance parameters extracted from the fits to the different channels are in good agreement. The fact that so similar results are obtained despite the very different appearance of the cross sections give a strong indication that the extracted parameters are correct. The values given in Table 3.2 are the weighted mean of the results from the three channels that were investigated.

Table 3.2: *Resonance parameters extracted from partial cross sections for the photodetachment of* K^-*. Present results are compared with the experimental results of Kiyan et al. [10] and the calculation of Liu [83].*

Present results		Kiyan *et al.*		Liu	
E_r (eV)	Γ (meV)	E_r (eV)	Γ (meV)	E_r (eV)	Γ (meV)
4.28(2)	44(20)	4.292(2)	10(2)	4.275 90	
4.294 68(9)	1.6(3)	4.294 5(1)	1.5(2)	4.294 72	1.472 2
		4.295 76(4)	0.10(8)	4.295 803 1	0.002
4.296 21(4)	0.28(5)	4.296 0(2)	0.30(3)	4.296 06	0.142 0
4.324(3)	22(5)			4.323 39	27.718 3
4.353 02(13)	1.72(12)			4.353 50	

3.4.1 Threshold modelling

The threshold behaviours in the K($5\,^2F$) and K($5\,^2G$) channels are shown in detail in Fig. 3.6. The shape of the threshold in the K($5\,^2F$) channel is similar to shapes that have been previously observed in photodetachment to residual atom states that have large positive dipole polarisabilities [43]. Liu calculated the polarisabilities of the $5\,^2F$ and $5\,^2G$ states to be 3.9×10^6 a.u. and -3.1×10^6 a.u., respectively [83]. In the presence of such large polarisabilities, cross sections are expected to deviate more than 20 % from the Wigner law at approximately 10 μeV above threshold [40]. In the present experiment, the Wigner law is not expected to describe the cross section above either of the two thresholds since its range of validity is less than the bandwidth of the laser used for photodetachment (25 μeV).

The threshold behaviour of the cross section in the K($5\,^2F$) channel can be explained by a simple semi-classical argument. The potential experienced by the detached electron is described by Eq. (1.1). With $\ell = 2$ and $\alpha = 3.9 \times 10^6$ a.u., the potential has a maximum at $r = 1145$ a.u. The height of the potential barrier is calculated to be 31 μeV. In the classical picture, the cross section is zero for energies below the barrier height, while above the barrier the cross section is fully developed. Such a simple model would predict a step in the cross section at 31 μeV above threshold. In a more sophisticated quantum mechanical treatment, however, tunnelling through the barrier needs to be considered. Tunnelling causes the onset of the cross section to coincide with the energetic threshold. In the quantum mechanical description, reflection of the electron wave at the barrier can still take place even when the electron energy is larger than the barrier height. The barrier is thus expected to influence the energy dependence of the cross section up

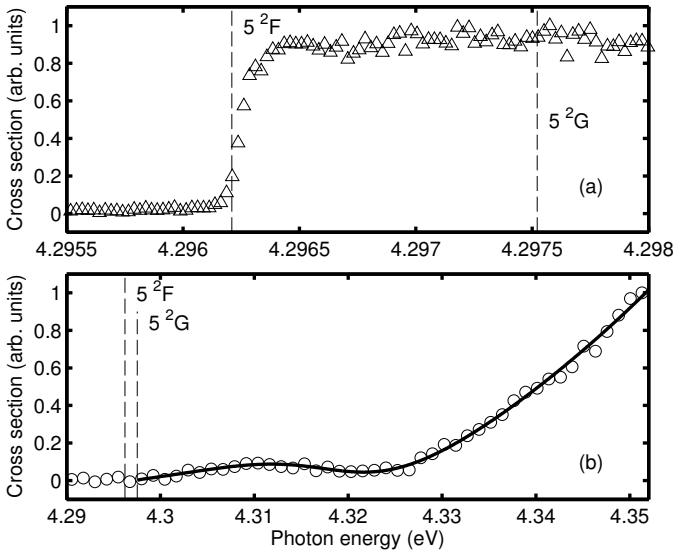

Figure 3.6: *The threshold behaviour in the* $\mathrm{K}(5\,^2F)$ *and* $\mathrm{K}(5\,^2G)$ *channels is shown in (a) and (b), respectively. In panel (b) the data is fit using Eq. (3.1). The non-resonant cross section is described by Eq. (3.7).*

to a few times the barrier height.

The cross section curve displayed in Fig. 3.6 (a) increases from zero to the maximum level within 200 μeV. It reaches the 80 % level at 100 μeV above threshold. This step-like behaviour in the $\mathrm{K}(5\,^2F)$ channel is thus in good agreement with the semi-classical argument above.

The threshold behaviour in the $\mathrm{K}(5\,^2G)$ channel represents the first observation of the influence of a dominant repulsive polarisation interaction in the final state. A semi-classical model was developed in order to qualitatively understand the shape of the cross section. The detached electron moves in the potential described by Eq. (1.1). For this kind of potential, the centrifugal part always dominates for large distances, while the induced dipole potential is most important at small distances. The borderline between the two regions is given by the point where the two potentials are of equal magnitude. In the case of the $5\,^2G$ state this occurs at 508 a.u. The total potential at this point is 1.3 meV, which means that the repulsive polarisation potential will have a dominating influence on the motion of the detached electron at energies above 1.3 meV. Most of the observed threshold data corresponds to electron energies above this value and so we neglect the centrifugal part of the potential in the model describing the energy dependence of the cross section. Due to the large repulsive potential, the classical turning point for

the free electron in the final state lies at a radius larger than 160 a.u. for the full energy range of the experiment. In the model we therefore assume that the only significant overlap between the initial state wavefunction and the free electron wavefunction is in the tunnelling region. The tunnelling wavefunction of the free electron can be expressed semi-classically in the form [84] (atomic units)

$$\psi_k(r) = \frac{C(E_e)}{r\sqrt{p(r)}} \exp\left(-\int_r^{r_0} p(x)\,dx\right), \tag{3.3}$$

where $k = (2E_e)^{1/2}$ is the linear momentum of the outgoing electron in the limit of large r, $p(r) = (|\alpha|/r^4 - 2E_e)^{1/2}$, $r_0 = (|\alpha|2E)^{1/4}$ is the classical turning point, and $C(E) \sim E^{-1/4}$ is a normalisation coefficient on the $k/2\pi$ momentum scale.

The integral in Eq. (3.3) has an analytical solution, which gives

$$\psi_k(r) = \frac{C(E_e)}{[|\alpha|(1 - r^4/r_0^4)]^{1/4}} \times \\ \times \exp\left(B(2E_e|\alpha|)^{1/4} - \frac{\sqrt{|\alpha|}}{r}\,{}_2F_1\left[-\frac{1}{2}, -\frac{1}{4}; \frac{3}{4}; \frac{r^4}{r_0^4}\right]\right), \tag{3.4}$$

where ${}_2F_1$ is a hypergeometric function and $B = (2\pi)^{3/2}/\Gamma^2(1/4) = 1.198$ is a numerical constant. By assuming that it is only the small radial distances that contribute to the overlap, the function can be expanded in $(r/r_0)^4$ around $r = 0$. The wavefunction takes the form

$$\psi_k(r) = E_e^{-1/4} \exp\left[B(2E_e|\alpha|)^{1/4}\right] \chi(r) \tag{3.5}$$

if only the first order terms in $(r/r_0)^4$ are considered. Here $\chi(r)$ depends on r but not on E_e. This separation of E_e and r dependencies is the key to calculating the energy dependence of the overlap between the initial and final state wavefunctions, which are denoted by Ψ_i and Ψ_f, respectively. Ψ_f is here represented by the product of ψ_k and the wavefunction for the residual atom in the $5\,{}^2G$ state. For a general transition operator, $\hat{V}$, the matrix element $\langle \Psi_f | \hat{V} | \Psi_i \rangle$ has an energy dependence that is simply given by the energy dependence of ψ_k. This follows from the fact that the only energy dependence in the matrix element is in ψ_k, for which the energy separation in Eq. (3.5) applies.

The cross section for photodetachment is given by an integral over the available phase space

$$\sigma_{\text{th}} \sim \int_{\mathbf{k}} \left|\langle \Psi_f | \hat{V} | \Psi_i \rangle\right|^2 \delta\left(\hbar\omega - EA_{\text{K}} - E_{5\,{}^2G} - E_e\right) \frac{d^3\mathbf{k}}{(2\pi)^3}, \tag{3.6}$$

where the δ-function ensures energy conservation. The phase space factor from the integral cancels the pre-exponential energy dependence from Eq. (3.5). The resulting threshold law is described by

$$\sigma_{\text{th}} \propto \exp\left(DE_e^{1/4}\right), \tag{3.7}$$

where $D = 2B(2|\alpha|)^{1/4}$.

The threshold model was successfully used to describe the non-resonant background in the K($5\,^2G$) channel. Good agreement between the model and the data in Figs. 3.5 and 3.2 were obtained. The energy and width of the resonance at 4.32 eV in the K($5\,^2G$) channel were also in good agreement with the resonance parameters obtained from both the K($7\,^2S$) and K($5\,^2F$) channels and the values calculated by Liu [83]. In paper **VI** it was discussed that the fit of the threshold model produces a value for the polarisability of the residual atom in the $5\,^2G$ state. The value obtained in this manner is about two orders of magnitude smaller than the theoretical value quoted by Liu [83]. We interpret this discrepancy as an indication that the semi-classical threshold model is an over simplification that is unable to describe all aspects of the threshold behaviour.

3.5 Caesium

In paper **VII**, photodetachment of Cs^- into the channels Cs($10\,^2S$), Cs($6\,^2F$) and Cs($6\,^2G$) was investigated. A major goal with the measurements was to observe similar threshold behaviours as was seen in K^- (paper **VI**). No prediction of the polarisability of the $6\,^2G$ state is available in the literature, but for $6\,^2F$ it has been calculated to be 7.77×10^6 a.u. [85]. The dipole polarisabilities of the two states can, however, be assumed to originate mainly from the interaction of the two states, since other states with $\Delta L = \pm 1$ are energetically far away. Moreover, the upper state in such an isolated pair always has a negative polarisability while the lower state has a positive polarisability. The polarisability of the $6\,^2G$ state can therefore be expected to be negative and of the same magnitude as the polarisability of the $6\,^2F$ state. With such large and negative polarisability, the threshold for the Cs($6\,^2G$) channel is expected to exhibit the same behaviour as was observed in the K($5\,^2G$) channel in paper **VI**.

Figure 3.7 shows the measured partial cross sections for the Cs($10\,^2S$), Cs($6\,^2F$) and Cs($6\,^2G$) channels. The cross sections start from their respective threshold and continue to above the Cs($10\,^2P_{3/2}$) channel opening. As can be seen in Fig. 3.7c, the threshold behaviour in the Cs($6\,^2F$) channel is similar to what was observed in the K($5\,^2F$) channel in K^- photodetachment.

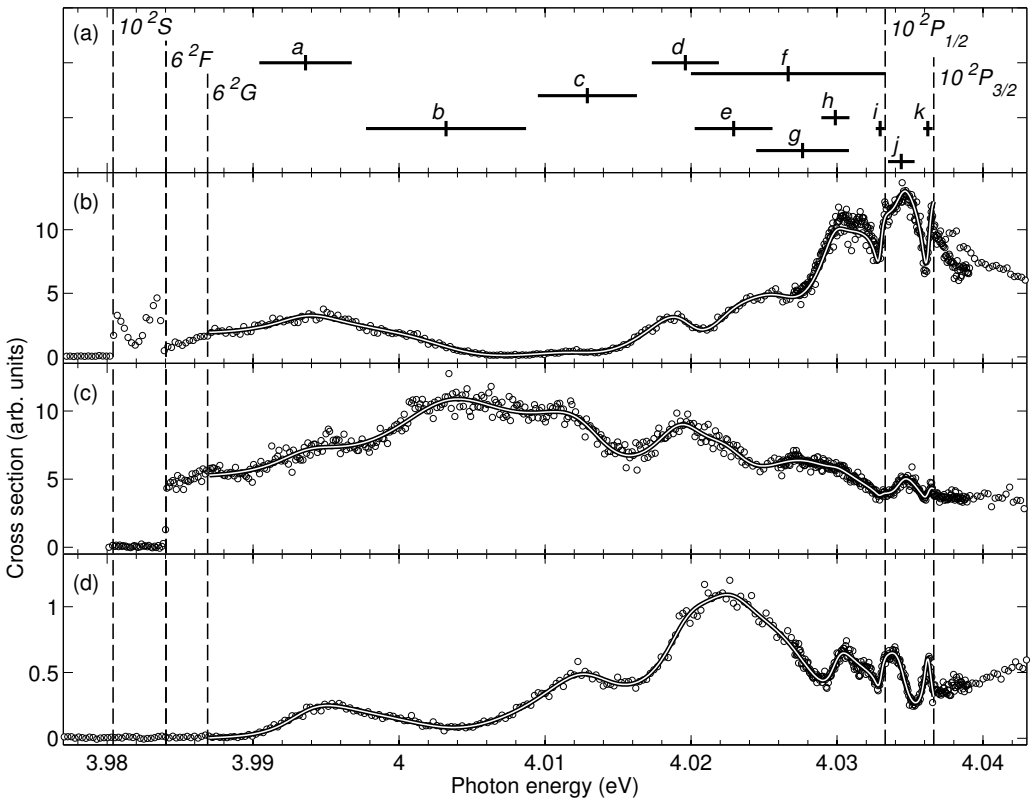

Figure 3.7: *Partial photodetachment cross sections in* Cs^-. *Panels (b), (c) and (d), show the* $Cs(10\,^2S)$, $Cs(6\,^2F)$ *and* $Cs(6\,^2G)$ *channels, respectively. The hollow lines show a fit of the model described in section 3.5.1. Panel (a) show the tentative resonance assignments from the fit. Channel openings are indicated with dashed lines.*

The onset of the cross section in the $Cs(6\,^2G)$ channel (Fig. 3.7d) is slow but any detailed investigations are hindered by the presence of many resonances in the region.

The cross sections shown in Fig. 3.7 have many distinct features. Some of the features line up well in all three channels. For example, the structure at approximately 4.036 eV, just below the opening of the $Cs(10\,^2P_{3/2})$ channel, is clearly seen in all three channels. In the region below the $Cs(10\,^2P_{1/2})$ channel opening, on the other hand, it is hard to point out the definitive position of any resonances. Further, it is difficult to extract resonance parameters from the data in Fig. 3.7, since many of the resonances are overlapping.

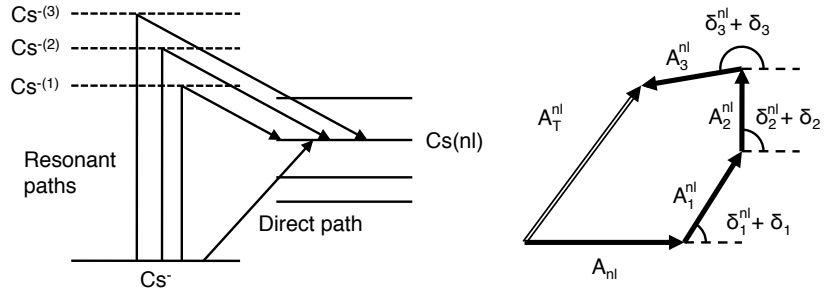

Figure 3.8: *Sketch of the simplified system used to describe interfering resonances.*

3.5.1 Fitting of overlapping resonances

A method to handle overlapping resonances is needed in order to extract energies and widths of resonances from the measured cross sections. The standard parameterisations [46, 86] describe only the interference between a single resonance and the non-resonant background. A numerical method that includes interference between multiple resonance is therefore deduced from a simplified description of the system. Figure 3.8 summarises the key concepts of this description. This corresponds to the simplest possible view of interfering resonances. A rigourous treatment of two interfering resonances in the presence of one open continuum is for example given by Friedrich [87]. The objective here is, however, not a complete description of the system, but rather to arrive at an expression that can be used to extract resonance parameters.

For a given photodetachment channel, Cs(nl) the reaction can proceed through multiple paths. First there is the direct path $\mathrm{Cs}^- + \gamma \rightarrow \mathrm{Cs}(nl) + e^-$, which is assigned an amplitude A_{nl}. The amplitude is given by the cross section for the non-resonant photodetachment process as $A_{nl} \propto \sqrt{\sigma_{pd}}$. Doubly excited states are described by their energy E_k and their width Γ_k. The presence of N doubly excited states opens up N additional paths

$$\mathrm{Cs}^- + \gamma \rightarrow \mathrm{Cs}^{-(k)} \rightarrow \mathrm{Cs}(nl) + e^-, \tag{3.8}$$

where $\mathrm{Cs}^{-(k)}$ are doubly excited states and $k = 1, 2, 3, \ldots, N$. Each path is assigned an amplitude A_k^{nl}, to which two different factors contribute. The first factor comes from the excitation of the negative ion to the state $\mathrm{Cs}^{-(k)}$. The excitation has a Lorentzian energy dependence, and thus

$$L_k \sim \frac{1}{\sqrt{{\epsilon_k}^2 + 1}} \tag{3.9}$$

holds for the excitation amplitude L_k, where $\epsilon_k = (\hbar\omega - E_k)/\frac{\Gamma_k}{2}$. The second factor of A_k^{nl} is the relative branching of the autodetaching decay of the DES. The decay proceeds to all states in Cs that lie below E_k and the relative population transferred to the state Cs(nl) is given by the coefficient B_{nl}^k. We now assume that the energy dependence of decay from $Cs^{-(k)}$ to the Cs(nl) is identical to the energy dependence of the non-resonant photodetachment amplitude from Cs^- to Cs(nl), e.i., $B_{nl}^k \propto A_{nl}$. With this assumption, for the otherwise unknown energy dependence of B_{nl}^k, a well known result can be obtained for a single resonances (see below).

So far, only the energy dependencies of L_k and B_{nl}^k have been considered. The absolute magnitudes of cross section for excitation and the branching in the decay are instead collected in the parameter s_k^{nl}, which describes the relative amplitude of the path via $Cs^{-(k)}$. With these parameters the resonance amplitude is given by

$$A_k^{nl} = L_k B_{nl}^k s_k^{nl} = \frac{s_k^{nl}\, A_{nl}}{\sqrt{{\epsilon_k}^2 + 1}}. \tag{3.10}$$

The amplitudes for the different paths can be added together, given that their relative phases are known. In this description the phase shifts have two parts. First, each resonant path has an intrinsic phase shift, δ_k^{nl}, compared to the direct path. Second, the excitation to a doubly excited state introduces an energy dependent phase shift of [87]

$$\delta_k = \arctan\left(-\frac{1}{\epsilon_k}\right). \tag{3.11}$$

With the above information it is possible to express the amplitude for photodetachment including the non-resonant cross section and the resonances as

$$A_T^{nl} = A_{nl} + \sum_{k=1}^{N} A_k^{nl} e^{i(\delta_k^{nl} + \delta_k)}, \tag{3.12}$$

and from this expression the cross section is give by $\sigma_T^{nl} \propto |A_T^{nl}|^2$.

This description of overlapping resonances should, of course, reproduce the established expression for an isolated resonance, when Eq. (3.12) is evaluated with $N = 1$. For a single resonance, the calculation of σ_T^{nl} can be performed analytically and gives the result

$$\sigma_T^{nl} \propto {A_{nl}}^2 \left(1 + \frac{-\epsilon\, 2\, s^{nl}\, \cos\left(\delta^{nl}\right) + \left(s^{nl}\right)^2 - 2\, s^{nl}\, \sin\left(\delta^{nl}\right)}{\epsilon^2 + 1}\right), \tag{3.13}$$

where the resonance index $k = 1$ have been dropped. By substituting $a = -2\,s^{nl}\cos(\delta^{nl})$ and $b = (s^{nl})^2 - 2\,s^{nl}\sin(\delta^{nl})$ into Eq. (3.13)

$$\sigma_T^{nl} \sim {A_{nl}}^2 \left(1 + \frac{\epsilon\, a + b}{\epsilon^2 + 1}\right) \tag{3.14}$$

is obtained, which is the well known form, for example given by [47]. The expression in Eq. (3.13) thus represents an alternative parameterisation giving the same result as the Shore [46] and Fano [86] profiles.

For more than one resonance, a simple analytical form cannot be obtained. It is, however, trivial to implement the calculation numerically by explicitly evaluating the terms of the sum in Eq. (3.12). The numerical expression can be used together with a standard fitting routine.

For the Cs data in Fig. 3.7, linear functions were used to describe the non-resonant cross sections in the Cs($10\,^2S$) and Cs($6\,^2F$) channels. In the Cs($6\,^2G$) channel, on the other hand, the threshold model in Eq. (3.7) was used, since a large negative polarisability was expected for the $6\,^2G$ state. The fitting was performed to all three data sets in Fig. 3.7 at the same time using 11 resonances. In this way it was possible to use the same energy, E_k, and width, Γ_k, for the resonance k in all the three channels. The strength, s_k^{nl}, and phase shift, δ_k^{nl}, were allowed to take different values in different channels. The result of the fit is shown as hollow lines in Fig. 3.7. The resonance parameters extracted from the fit are indicated in Fig. 3.7a and are given in Table 3.3.

The resonance identifications made with this fit are only tentative. Some of the assignment of resonances are, however, more plausible than others. The resonances *i*, *j* and *k* can clearly be seen in all three channels. The parameters extracted for these resonates can thus be considered to be rather reliable. In the region of resonances *a* and *b*, below 4.01 eV, it seems like two

Table 3.3: *Resonance parameters extracted from a fit to the data in Fig 3.7. Uncertainties represent one sigma confidence interval in the fit.*

Label	E_r (eV)	Γ (meV)	Label	E_r (eV)	Γ (meV)
a	3.093 6(4)	6.3(7)	*g*	4.027 6(18)	6.0(40)
b	4.003 2(6)	11.0(12)	*h*	4.029 89(22)	1.9(5)
c	4.012 9(6)	6.8(12)	*i*	4.032 96(5)	0.61(9)
d	4.019 6(5)	4.6(10)	*j*	4.034 40(14)	1.8(3)
e	4.022 9(14)	5.3(2.6)	*k*	4.036 22(4)	0.65(1)
f	4.027(5)	13(9)			

resonances are enough to reproduce the observed structures. Between 4.01 eV and the Cs($10\,^2P_{1/2}$) channel opening, it is clear that several resonances are needed to reproduce the modulations in the three channels. The assignment of resonance parameters might, however, have many different solutions depending on the resonance model and the functional form of the non-resonant cross section. As mentioned above, the identification of resonance i is reliable whereas the assignment of resonances c to h is very tentative. It is not even clear how many resonances that is causing the structure in this energy range. Comparisons of the experimental cross sections with results of *ab initio* calculations would be needed in order to obtain a clear description of the observed resonance structure.

CHAPTER 4

Conclusions and outlook

The most important scientific outcome of this thesis is the first observation of a photodetachment threshold for a channel in which the residual atom is left in an excited state with a large negative polarisability (paper **VI**). The selective detection of highly excited final state atoms, as described in paper **V** was the key to the success of this measurement. The large resonance modulations in the K($7\,^2S$) channel, compared to the K($5\,^2S$) channel, is an example of the advantages of detecting highly excited residual atoms. The measurements described in papers **V** and **VII** also illustrates the value of observing the same resonances in several different final state channels. This makes it possible to compare resonance parameters in cases where the non-resonant cross sections and the resonance shapes might be different. Such a procedure results in a more reliable determination of the resonance parameters. If only a single channel is used, an incorrect description of the non-resonant background could significantly change the values of the resonance parameters.

Papers **V**, **VI** and **VII** present the first results from experiments with the new detection scheme. The work described in these papers mark the beginning of a series of experiments designed to investigate doubly excited states that are increasingly more excited. The ultimate goal is to reach the double detachment limit. The present state selective detection scheme, which is based on resonance ionisation, should allow us to investigate final state channels in which the valence electron of the residual atom is bound by more than 0.3 eV. This would, for example, correspond to the K($7\,^2D$) channel in K^- photodetachment. Detection of higher channels is possible if

the final state neutral atom can be directly field ionised without the resonant excitation. In such an experiment it would be possible to investigate multiple channels simultaneously, as long as the excited states of the residual atom can be resolved. The major improvement that is needed to perform this kind of experiments is a Rydberg state analyser with very high selectivity. Currently, positive ions resulting from the field ionisation of a particular Rydberg state can be well separated from those ions that are produced prior to the field ioniser. The spot size on the detector is, however, larger than the separation between adjacent Rydberg states. Two states with a small energy separation can therefore not be separated with the current field ioniser.

An important aspect of the recent improvement of the experimental capabilities was the upgrade of the ion beam apparatus at GUNILLA. This improvement provided a much better mass resolution, with maintained transmission through the interaction region (paper **I**). As a result, it was possible to perform some interesting measurements on heavy atomic negative ions. In paper **IV** an unambiguous identification of the $^2S_{1/2}$ state in Pt^- was presented. The measured binding energy of the $^2S_{1/2}$ state was significantly different from the predictions of Thøgersen *et al.* [80] and Zollweg [81]. This discrepancy indicates that the theoretical models are presently not capable of predicting accurate term splittings in heavy negative ions.

The measurement on W^- resulted in a reduction of the uncertainty in the electron affinity by a factor of 50. Moreover, the detachment signal observed at photon energies below the ground state threshold was identified with detachment from a previously unknown excited state in W^-. This identification would not have been possible without the high mass resolution of the upgraded apparatus.

The experiment described in paper **II** demonstrated that high resolution photodetachment measurements in the infrared can be performed with pulsed OPOs. The work provided significantly better values for the EA of potassium and the fine structure splitting in P^-. The agreement between the measured EA and the value calculated by de Oliveira *et al.* [78], indicates the latter is indeed correct at the 100 μeV level.

The main motivation for this work was that through studies of negative ions we could learn something about electron-electron correlation. The largest contribution in this direction have so far been the interpretation of the photodetachment threshold to a state with large and negative polarisability. For most of the other experiments, the results on their own does not teach us that much. In many cases, it is first when the experimental results are compared to calculations that the physics behind can be understood. With the experimental capabilities that now exists at GUNILLA, new regions of experiments can be accessed. I hope that the new capabilities and the new

results will trigger more theoretical work in the subject of negative ions.

There are many interesting future directions for experiments in this field. For example, the use of the photodetachment process to suppress isobaric interferences in mass spectrometry. This will require detailed studies of the binding energies of the atomic and molecular negative ions of interest. Moreover, new laboratory investigations will be needed to interpret the latest observations of negative ions in the interstellar media. Experiments designed to address problems in both these fields will require high mass resolution and good transmission, which is now available at the ion beam apparatus at GUNILLA.

Future research most related to my thesis work is, of course, the continuation of investigations of highly excited states in negative ions. One of the original goals with the development of the detection system was to enable measurements of the threshold cross section for double detachment. Beyond this threshold, positive ions will constitute the double detachment signal. In such experiments, however, there will always be a background contribution from field ionised Rydberg atoms. It would be expected that this background contribution could be reduced and quantified by the use of an improved Rydberg state analyser. By tuning the photon energy across the limit for double detachment, the branching ratios for population of different Rydberg states of the atom could be directly measured. Experimental studies in this energy regime would be explorations on the border between states with two excited electrons and a continuum of two free electrons.

Acknowledgements

I don't think you can get anywhere close to writing a Ph.D. thesis on your own. I would not be at this point without the work and support of many people. I would like to mention some of these by name.

My supervisor, Prof. Dag Hanstorp, made all this possible by employing me as a Ph.D. student. Without his expertise in physics and his experimental skills I would be far from where I am today. Prof. Ann-Marie Mårternsson-Pendrill has been my examiner for the last two years, and has given me valuable support. Dr. Pontus Andersson, my former office mate and member of the negative ion group, got the task of introducing me to the laboratory. He did a splendid job, and managed to put up with my endless questions. M.Sc. Johan Rohlén brought new knowledge and fun when he joined the group. His programming skills have been vital for the project.

Without the expertise of Jan-Åke Wiman in the workshop, the ion beam apparatus would not be in as good shape as it is. However, no experiments are possible without ions, and there would have been no ions without our chemist, Heinrich Riedl. Mats Rostedt has been instrumental in handling technical, electronic and computer-related problems in the lab.

A frequent visitor in Göteborg, Prof. David Pegg, has had a great influence on my work. We have had many interesting discussions and a lot of fun, in the lab and outside. Prof. Wesley Walter, Prof. Igor Kiyan and M.Sc. Hannes Hultgren have all payed important roles throughout the experiments, taking part in preparations, performing calculations, and interpreting results are only a few of them.

Prof. Klavs Hansen and Prof. Sten Salomonson have gladly shared their knowledge on physics. So have my fellow Ph.D. students Erika, Săsa, Niklas, Mikael, Gustav and Robert, we have also had much fun together.

My schoolteacher in 4^{th}–6^{th} grades, Marja Claesson, opened my eyes to mathematics and made me understand it is not all about numbers. Without

her influence I would probably have been someone completely different today.

My parents, Maria and Johnny, have always supported me. As mentioned in the preface, it seems they set me on this track already in early years.

These are some of the people who have contributed, in different ways, on my path to this thesis. The most important person, however, is my wife Lina. What she means to me cannot be captured on paper.

Bibliography

[1] W. Klopper, R. A. Bachorz, D. P. Tew, and C. Hättig. *Phys. Rev. A* 81: 022503 (2010)

[2] K. R. Lykke, K. K. Murray, and W. C. Lineberger. *Phys. Rev. A* 43: 6104 (1991)

[3] E. Lindroth and J. L. Sanz-Vicario. *Radiat. Phys. Chem.* 70: 387 (2004)

[4] H. R. Sadeghpour and C. H. Greene. *Phys. Rev. Lett.* 65: 313 (1990)

[5] M. K. Raarup, U. V. Pedersen, V. V. Petrunin, P. Balling, and T. Andersen. *Phys. Rev. Lett.* 85: 4028 (2000)

[6] P. G. Harris, H. C. Bryant, A. H. Mohagheghi, R. A. Reeder, H. Sharifian, *et al. Phys. Rev. Lett.* 65: 309 (1990)

[7] U. Ljungblad, D. Hanstorp, U. Berzinsh, and D. J. Pegg. *Phys. Rev. Lett.* 77: 3751 (1996)

[8] G. Haeffler, I. Y. Kiyan, U. Berzinsh, D. Hanstorp, N. Brandefelt, *et al. Phys. Rev. A* 63: 053409 (2001)

[9] G. Haeffler, I. Y. Kiyan, D. Hanstorp, B. J. Davies, and D. J. Pegg. *Phys. Rev. A* 59: 3655 (1999)

[10] I. Y. Kiyan, U. Berzinsh, J. Sandström, D. Hanstorp, and D. J. Pegg. *Phys. Rev. Lett.* 84: 5979 (2000)

[11] V. V. Petrunin, M. H. Jacobsen, L. B. Madsen, S. A. Aseyev, and T. Andersen. *Phys. Rev. Lett.* 90: 013002 (2003)

[12] A. E. Klinkmüller, G. Haeffler, D. Hanstorp, I. Y. Kiyan, U. Berzinsh, *et al. Phys. Rev. A* 56: 2788 (1997)

[13] J. J. Thomson. *P. Roy. Soc. A: Math. Phy.* 89: 1 (1913)

[14] R. Wildt. *Astrophys. J.* 90: 611 (1939)

[15] R. Wildt. *Astropys. J.* 93: 47 (1941)

[16] L. M. Branscomb and S. J. Smith. *Phys. Rev.* 98: 1028 (1955)

[17] L. M. Branscomb and W. L. Fite. *Phys. Rev.* 93: 651 (1954)

[18] L. M. Branscomb and S. J. Smith. *Phys. Rev.* 98: 1127 (1955)

[19] H. Massey. *Negative ions*. 3rd edition. Cambridge university press (1976)

[20] T. Andersen, H. K. Haugen, and H. Hotop. *J. Phys. Chem. Ref. Data* 28: 1511 (1999)

[21] J. Rienstra-Kiracofe, G. Tschumper, H. Schaefer, S. Nandi, and G. Ellison. *Chem. Rev.* 102: 231 (2002)

[22] M. Draghici and E. Stamate. *J. Appl. Phys.* 107: 123304 (2010)

[23] S. Knist, F. Greiner, F. Biss, and A. Piel. *Contrib. Plasm. Phys.* 51: 769 (2011)

[24] A. Kojima, M. Hanada, Y. Tanaka, M. Kawai, N. Akino, *et al. Nucl. Fusion* 51: 083049 (2011)

[25] R. Hemsworth, H. Decamps, J. Graceffa, B. Schunke, M. Tanaka, *et al. Nucl. Fusion* 49: 045006 (2009)

[26] W. Kutschera. *Int. J. Mass. Spectrom.* 242: 145 (2005)

[27] D. Nelson, R. Korteling, and W. Stott. *Science* 198: 507 (1977)

[28] H. Kjennbakken, H. P. Sejrup, and H. Haflidason. *Holocene* 21: 897 (2011)

[29] E. Roueff and E. Herbst. *J. Phys. Conf. Ser.* 192: 012008 (2009)

[30] E. Herbst and W. Klemperer. *Astrophys. J.* 185: 505 (1973)

[31] M. C. McCarthy, C. A. Gottlieb, H. Gupta, and P. Thaddeus. *Asrophys. J. Lett.* 652: L141 (2006)

[32] P. Andersson, O. Forstner, D. Hanstorp, A. O. Lindahl, and K. Wendt. *AIP Conf. Proc.* 1104: 53 (2009)

[33] W. M. Haynes, editor. *CRC Handbook of Chemistry and Physics.* 91st edition. CRC Press/Taylor and Francis, Boca Raton, FL (Internet Version 2011)

[34] R. C. Bilodeau and H. K. Haugen. *Phys. Rev. Lett.* 85: 534 (2000)

[35] U. Warring, M. Amoretti, C. Canali, A. Fischer, R. Heyne, *et al. Phys. Rev. Lett.* 102: 043001 (2009)

[36] C. W. Walter, N. D. Gibson, C. M. Janczak, K. A. Starr, A. P. Snedden, *et al. Phys. Rev. A* 76: 052702 (2007)

[37] E. P. Wigner. *Phys. Rev.* 73: 1002 (1948)

[38] R. C. Bilodeau, M. Scheer, and H. K. Haugen. *Phys. Rev. Lett.* 87: 143001 (2001)

[39] J. W. Farley. *Phys. Rev. A* 40: 6286 (1989)

[40] T. F. O'Malley. *Phys. Rev.* 137: A1668 (1965)

[41] H. Hotop and W. C. Lineberger. *J Chem. Phys.* 58: 2379 (1973)

[42] H. Hotop, T. A. Patterson, and W. C. Lineberger. *Phys. Rev. A* 8: 762 (1973)

[43] J. Sandström, G. Haeffler, I. Kiyan, U. Berzinsh, D. Hanstorp, *et al. Phys. Rev. A* 70: 052707 (2004)

[44] S. Watanabe and C. H. Greene. *Phys. Rev. A* 22: 158 (1980)

[45] S. J. Buckman and C. W. Clark. *Rev. Mod. Phys.* 66: 539 (1994)

[46] B. W. Shore. *Phys. Rev.* 171: 43 (1968)

[47] C.-N. Liu and A. F. Starace. *Phys. Rev. A* 60: 4647 (1999)

[48] C. Blondel, C. Delsart, and F. Dulieu. *Phys. Rev. Lett.* 77: 3755 (1996)

[49] C. Blondel, W. Chaibi, C. Delsart, C. Drag, F. Goldfarb, and S. Kroger. *Eur. Phys. J. D* 33: 335 (2005)

[50] S. J. Cavanagh, S. T. Gibson, M. N. Gale, C. J. Dedman, E. H. Roberts, and B. R. Lewis. *Phys. Rev. A* 76: 052708 (2007)

[51] D. W. MacArthur, K. B. Butterfield, D. A. Clark, J. B. Donahue, P. A. M. Gram, *et al. Phys. Rev. A* 32: 1921 (1985)

[52] G. Haeffler, D. Hanstorp, I. Kiyan, A. E. Klinkmüller, U. Ljungblad, and D. J. Pegg. *Phys. Rev. A* 53: 4127 (1996)

[53] M. Allan, O. Zatsarinny, and K. Bartschat. *J. Phys. B: At. Mol. Opt. Phys.* 44: 065201 (2011)

[54] L. Vejby-Christensen, D. Kella, D. Mathur, H. B. Pedersen, H. T. Schmidt, and L. H. Andersen. *Phys. Rev. A* 53: 2371 (1996)

[55] K. Fritioff, J. Sandstrom, P. Andersson, D. Hanstorp, F. Hellberg, *et al. Phys. Rev. A* 69: 042707 (2004)

[56] K. Fritioff, J. Sandström, P. Andersson, D. Hanstorp, F. Hellberg, *et al. J. Phys. B: At. Mol. Opt. Phys.* 37: 2241 (2004)

[57] H. B. Pedersen, N. Djurić, M. J. Jensen, D. Kella, C. P. Safvan, *et al. Phys. Rev. A* 60: 2882 (1999)

[58] D. S. Walton, B. Peart, and K. Dolder. *J. Phys. B: At. Mol. Phys.* 3: L148 (1970)

[59] D. S. Walton, B. Peart, and K. T. Dolder. *J. Phys. B: At. Mol. Phys.* 4: 1343 (1971)

[60] L. H. Andersen, D. Mathur, H. T. Schmidt, and L. Vejby-Christensen. *Phys. Rev. Lett.* 74: 892 (1995)

[61] M. O. A. El Ghazaly, A. Svendsen, H. Bluhme, A. B. Nielsen, S. B. Nielsen, and L. H. Andersen. *Phys. Rev. Lett.* 93: 203201 (2004)

[62] O. Aviv, Y. Toker, D. Strasser, M. L. Rappaport, O. Heber, *et al. Phys. Rev. A* 83: 023201 (2011)

[63] P. Hlavenka, R. Otto, S. Trippel, J. Mikosch, M. Weidemüller, and R. Wester. *J. Chem. Phys.* 130: 061105 (2009)

[64] N. Berrah, J. D. Bozek, A. A. Wills, G. Turri, H.-L. Zhou, *et al. Phys. Rev. Lett.* 87: 253002 (2001)

[65] I. Dumitriu, R. C. Bilodeau, T. W. Gorczyca, C. W. Walter, N. D. Gibson, *et al. Phys. Rev. A* 81: 053404 (2010)

[66] J. C. Bopp, J. R. Roscioli, M. A. Johnson, T. M. Miller, A. A. Viggiano, *et al. J. Phys. Chem. A* 111: 1214 (2007)

[67] W. Eisfeld. *J. Chem. Phys.* 134: 054303 (2011)

[68] D. Hanstorp. *Nucl. Instrum. Meth. B* 100: 165 (1995)

[69] P. Juncar, C. R. Bingham, J. A. Bounds, D. J. Pegg, H. K. Carter, *et al. Phys. Rev. Lett.* 54: 11 (1985)

[70] P. Defrance, F. Brouillard, W. Claeys, and G. V. Wassenhove. *J. Phys. B: At. Mol. Phys.* 14: 103 (1981)

[71] J. J. Blangé, X. Urbain, H. Rudolph, H. A. Dijkerman, H. C. W. Beijerinck, and H. G. M. Heideman. *J. Phys. B: At. Mol. Opt. Phys.* 29: 2763 (1996)

[72] A. M. Covington, A. Aguilar, I. R. Covington, M. F. Gharaibeh, G. Hinojosa, *et al. Phys. Rev. A* 66: 062710 (2002)

[73] H. Bruhns, H. Kreckel, K. Miller, M. Lestinsky, B. Seredyuk, *et al. Rev. Sci. Instrum.* 81 (2010)

[74] S. Kaufman. *Opt. Commun.* 17: 309 (1976)

[75] J. Ederth, P. Johnsson, G. A. Niklasson, A. Hoel, A. Hultåker, *et al. Phys. Rev. B* 68: 155410 (2003)

[76] D. Feldmann. *Z. Phys. A: Hadron. Nucl.* 277: 19 (1976)

[77] J. Slater and W. C. Lineberger. *Phys. Rev. A* 15: 2277 (1977)

[78] G. de Oliveira, J. M. L. Martin, F. de Proft, and P. Geerlings. *Phys. Rev. A* 60: 1034 (1999)

[79] R. C. Bilodeau, M. Scheer, H. K. Haugen, and R. L. Brooks. *Phys. Rev. A* 61: 012505 (1999)

[80] J. Thögersen, M. Scheer, L. D. Steele, H. K. Haugen, and W. P. Wijesundera. *Phys. Rev. Lett.* 76: 2870 (1996)

[81] R. J. Zollweg. *J. Chem. Phys.* 50: 4251 (1969)

[82] A. A. Bengali, S. M. Casey, C. L. Cheng, J. P. Dick, P. T. Fenn, *et al. J. Am. Chem. Soc.* 114: 5257 (1992)

[83] C.-N. Liu. *Phys. Rev. A* 64: 052715 (2001)

[84] L. D. Landau and E. M. Lifshitz. *Quantum Mechanics. Non-relativistic Theory.* 3rd edition. Pergamon, Oxford (1977)

[85] W. van Wijngaarden and J. Li. *J. Quant. Spectrosc. Ra.* 52: 555 (1994)

[86] U. Fano. *Phys. Rev.* 124: 1866 (1961)

[87] H. Friedrich. *Theoretical atomic physics.* Springer, Berlin (1991)